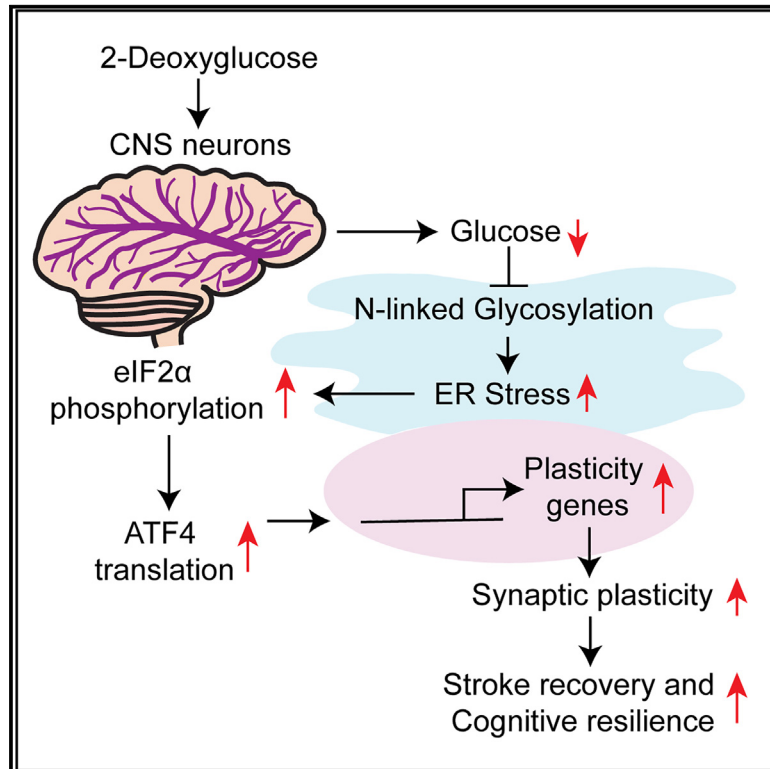# 2-Deoxyglucose drives plasticity via an adaptive ER stress-ATF4 pathway and elicits stroke recovery and Alzheimer's resilience

Graphical abstract

Authors

Amit Kumar,
Saravanan S. Karuppagounder,
Yingxin Chen, ..., Tõnis Timmusk,
Daniel H. Geschwind, Rajiv R. Ratan

Correspondence

rrr2001@med.cornell.edu

In brief

Intermittent fasting (IF) is a nutritional paradigm that forestalls cognitive aging, stroke disability, and Alzheimer's progression. How glucose restriction, an aspect of IF, contributes to IF-induced benefits is unclear. Here, we used 2-deoxyglucose to elucidate how low glucose engages an evolutionarily conserved ER stress response pathway to stimulate brain plasticity and treat stroke and AD.

Highlights

- 2-deoxyglucose (2-DG), a glucose-restriction mimetic, drives *Bdnf* transcription

- 2-DG reduces disability after ischemic stroke and improves cognition in AD

- 2-DG inhibits N-glycosylation to induce ER stress, ATF4, and *Bdnf* transcription

- N-glycosylation senses low glucose to drive adaptation to stroke and AD

CellPress

Article

2-Deoxyglucose drives plasticity via an adaptive ER stress-ATF4 pathway and elicits stroke recovery and Alzheimer's resilience

Amit Kumar,[1] Saravanan S. Karuppagounder,[1] Yingxin Chen,[1] Carlo Corona,[1] Riki Kawaguchi,[2] Yuyan Cheng,[2] Mustafa Balkaya,[1] Botir T. Sagdullaev,[1,3] Zhexing Wen,[5] Charles Stuart,[6] Sunghee Cho,[1] Guo-li Ming,[7] Jürgen Tuvikene,[4] Tõnis Timmusk,[4] Daniel H. Geschwind,[2] and Rajiv R. Ratan[1,8,*]

[1]Burke Neurological Institute and Brain and Mind Research Institute, Weill Cornell Medicine, 785 Mamaroneck Ave, White Plains, NY, USA
[2]Department of Neurology, David Geffen School of Medicine, University of California, Los Angeles, Los Angeles, CA 90095, USA
[3]Regeneron Pharmaceuticals, Tarrytown, New York, NY, USA
[4]Department of Chemistry and Biotechnology, Tallinn University of Technology, Tallinn, Estonia
[5]Departments of Psychiatry and Behavioral Sciences, Cell Biology, and Neurology, Emory University School of Medicine, Atlanta, GA, USA
[6]East Tennessee State University Quillen College of Medicine, Johnson City, TN, USA
[7]Department of Neuroscience, Perelman School for Medicine, University of Pennsylvania, Philadelphia, PA, USA
[8]Lead contact
*Correspondence: rrr2001@med.cornell.edu
https://doi.org/10.1016/j.neuron.2023.06.013

SUMMARY

Intermittent fasting (IF) is a diet with salutary effects on cognitive aging, Alzheimer's disease (AD), and stroke. IF restricts a number of nutrient components, including glucose. 2-deoxyglucose (2-DG), a glucose analog, can be used to mimic glucose restriction. 2-DG induced transcription of the pro-plasticity factor, *Bdnf*, in the brain without ketosis. Accordingly, 2-DG enhanced memory in an AD model (5xFAD) and functional recovery in an ischemic stroke model. 2-DG increased *Bdnf* transcription via reduced N-linked glycosylation, consequent ER stress, and activity of ATF4 at an enhancer of the *Bdnf* gene, as well as other regulatory regions of plasticity/regeneration (e.g., *Creb5*, *Cdc42bpa*, *Ppp3cc*, and *Atf3*) genes. These findings demonstrate an unrecognized role for N-linked glycosylation as an adaptive sensor to reduced glucose availability. They further demonstrate that ER stress induced by 2-DG can, in the absence of ketosis, lead to the transcription of genes involved in plasticity and cognitive resilience as well as proteostasis.

INTRODUCTION

Brain aging and age-associated neurological diseases such as Alzheimer's disease (AD) begin decades before their symptoms manifest.[1–3] Identifying dietary manipulations that forestall these changes could provide ways to limit the growing epidemic of disabilities from age-associated neurological conditions.

Intermittent fasting (IF) is a dietary intervention widely implicated in improving brain health, cognitive aging, AD, and stroke. During the fasting phase, glycogen stores are depleted, leading to low circulating glucose levels and a metabolic switch triggering adipose cells to release fatty acids to the liver where they are converted to ketone bodies.[4,5] Reducing glucose and increasing ketone bodies via IF improves brain physiology and pathology. IF regimens show significant cognitive improvement in healthy aged mice.[6,7] Moreover, rodent models of AD show significant IF-induced cognitive improvements.[8–10] These studies demonstrate IF as an effective strategy for improving cognition in aged mice with AD.

Human studies also show beneficial effects on cognitive function. In an elderly population with mild cognitive impairment, a precursor of AD, IF diminished the progression of memory decline.[11] Among older Italian adults, individuals adherent to IF were less likely to have cognitive impairment than those with no eating time restrictions.[12] These studies suggest that despite distinct protocols, IF may result in cognition benefits. However, animal and human studies have been hampered by a lack of understanding of the precise target(s) for IF-mediated improvements in cognition.

The metabolic switch from glucose to ketone utilization is considered one driver of the beneficial effects of IF on the brain.[13] In the fasting state, ketone bodies both provide an alternative energy fuel and drive resilience via signaling molecules. β-Hydroxybutyrate (BHB) activates the SIRT3/PGC1α/UCP2 pathway, which stimulates mitochondrial biogenesis,[14] blocks NLRP3 inflammasome,[15] and induces autophagy.[16] BHB upregulates the expression of brain-derived neurotrophic factor (BDNF)[17,18] by inhibiting repressive HDAC2 and HDAC3 binding on *Bdnf* promoter.[18]
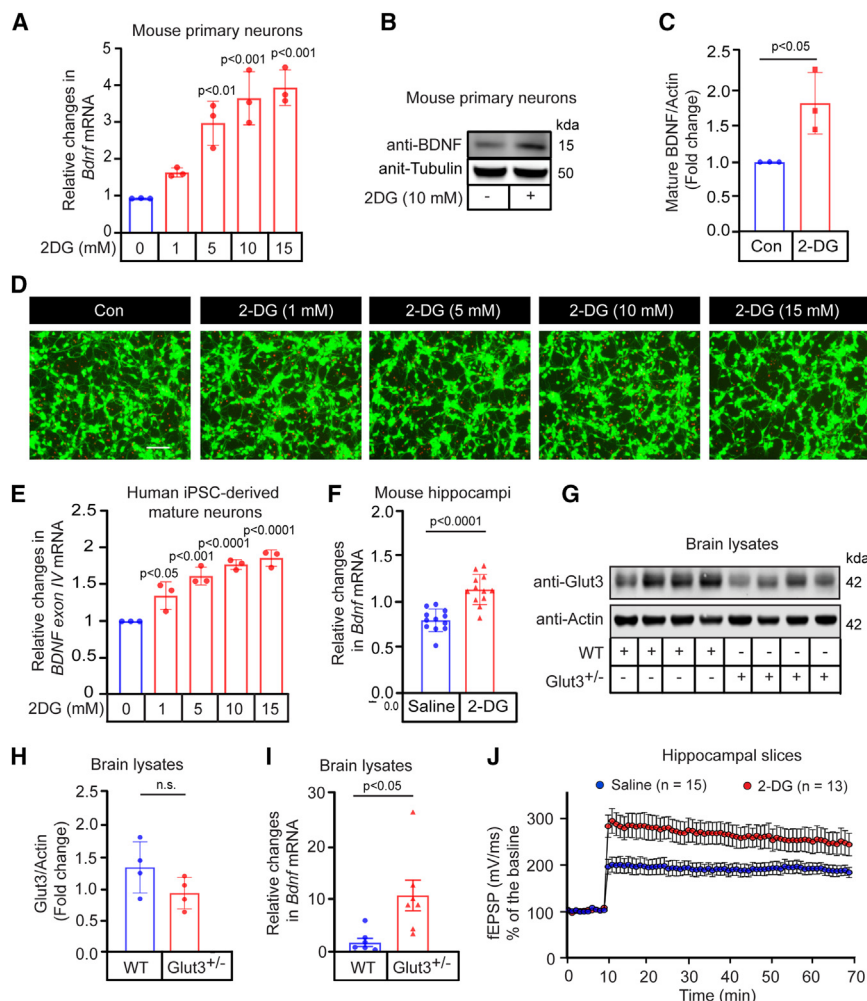
Figure 1. 2-DG induces *Bdnf* message and LTP without affecting neuronal viability

(A) 2-DG treatment for 6 h in mouse neurons (2 DIV) (n = 3, mean ± SD, one-way ANOVA with Dunnett post hoc test).

(B and C) 2-DG treatment for 6 h in mouse neurons (2 DIV) (n = 3, mean ± SD, Student's t test).

(D) Live (green, calcein-acetoxymethyl ester [AM] stain)-dead (red, ethidium homodimer) staining of mouse neurons treated with 2-DG for 24 h (scale bars, 50 μm, n = 3 independent cultures).

(E) 2-DG treatment for 6 h in human iPSC-derived cortical neurons (n = 3, mean ± SD, one-way ANOVA with Dunnett post hoc test).

(F) 2-DG (10 mg/kg) i.p. injection for 6 h (mean ± SEM, Student's t test).

(G and H) Glut3 immunoblot in lysates from wild-type (WT) and Glut3 heterozygous knockout (Glut3$^{+/-}$) mice brain cortices (mean ± SEM, Student's t test).

(I) BDNF message levels in brain cortices of 3-month-old Glut3$^{+/-}$ and WT mice (mean ± SEM, Student's t test).

(J) LTP elicited by 3 × theta-bursts in hippocampal slices submerged either in ACSF alone (vehicle) or in ACSF with 10 mM 2-DG for 6 h. For statistical details, see Table S2.

2-DG resulted in a concentration-dependent increase in the message levels of *Bdnf* (Figure 1A). Like 2-DG, lowering extracellular glucose increased *Bdnf* message levels in a concentration-dependent manner (Figures S4A and S4G). Further, 2-DG treatment for 24 h significantly increased mature BDNF protein (Figures 1B and 1C).

To verify that increases in BDNF were not a response to 2-DG toxicity, we monitored cell viability. Live-dead staining showed no increased cell death after 24 h of 2-DG exposure (Figure 1D). To determine whether 2-DG-induced *Bdnf* expression occurs through BHB, we measured its levels following treatment with 10 mM 2-DG for 8 h, a time when *Bdnf* mRNA was induced. 2-DG did not increase BHB levels (Figure S1A), suggesting that low glucose increased BDNF via ketone-independent pathways in cultured neurons.

Potassium chloride (KCl)-potentiated depolarization induces *Bdnf* gene expression in cortical neurons.[28,29] Accordingly, we determined whether 2-DG depolarizes neurons to increase *Bdnf* expression. Primary cortical neurons (2-DIV) with 2-DG were assessed for *Bdnf* induction in the presence or absence of KCl (25 mM). Sodium chloride (NaCl, 25 mM) was used as an osmolarity control. 2-DG increased *Bdnf* gene expression in a concentration-dependent manner identically with and without KCl-induced depolarization, suggesting that 2-DG does not induce depolarization to induce *Bdnf* (Figure S1B).

At 2-DIV, mouse cortical neurons do not express glutamate receptors and are not synaptically active.[30] To address whether glutamatergic, synaptically active human neurons respond to

The beneficial effects of low glucose, beyond its inducing ketogenesis for cognition and resilience, are relatively understudied. We explored the effects of 2-deoxyglucose (2-DG),[3,19] which inhibits the utilization of glucose by blocking its transport and metabolism.[20–23] We leveraged *in vitro* and *in vivo* models to show that 2-DG enhances BDNF expression. Using BDNF expression rather than ketone formation as a biomarker for dosing 2-DG, we demonstrate that 2-DG could treat memory dysfunction in an AD model and enhance recovery in an ischemic stroke model at a concentration that increases the expression of *Bdnf*. 2-DG induced sublethal endoplasmic reticulum (ER) stress, resulting in ATF4-driven expression of BDNF and other plasticity-associated genes.

RESULTS

2-Deoxyglucose induces BDNF mRNA and protein in cortical neurons

2-DG inhibits or enhances BDNF expression.[24,25] BDNF plays roles in plasticity and cognitive improvement.[26,27] To evaluate the relationship between 2-DG and levels of *Bdnf*, we used qPCR to monitor mRNA levels 6 h after treatment. The treatment of cortical neurons (2 days *in vitro* [2-DIV]) with

2-DG by increasing *BDNF*, we utilized human induced pluripotent stem cells (iPSCs) differentiated first into forebrain progenitors and then into MAP2 ab+ neurons (>99%). About 90% of the neurons in this protocol were glutamatergic, as demonstrated by vesicular glutamate transporter 1 (VGLUT1) and Ca^{2+}-calmodulin-dependent protein kinase 2 (CaMKII) positivity.[31] We examined the expression of *BDNF exon IV* in response to 2-DG. 2-DG treatment for 6 h showed a concentration-dependent increase in *Bdnf* message (Figure 1E). Thus, like synaptically inactive mouse neurons, 2-DG treatment enhances *Bdnf* gene expression in synaptically active human neurons.

We next asked whether 2-DG induces *Bdnf* gene expression in the brains of living mice. We injected 8- to 10-week-old C57BL/6 mice intraperitoneally (i.p.) with different doses of 2-DG (10, 50, 100 mg/kg) for 6 h (dose range based on a rodent study where 2-DG at $\geq$200 mg/kg showed behavioral side effects[32]). 2-DG at 10 mg/kg led to a significant increase in *Bdnf* gene expression, whereas 50 mg/kg did not; and 100 mg/kg showed a non-significant upward trend (Figures 1F and S1C).

Because a consequence of 2-DG treatment is reduced glucose utilization in cultured neurons, we examined whether germline reduction of Glut3, a glucose transporter dominant in neurons, increases *Bdnf* levels in mice. We compared *Bdnf* expression levels in brain cortical samples of 3-month-old wild-type (WT) and heterozygous knockout mice (Glut3$^{+/-}$). Homozygous knockout mice (Glut3$^{-/-}$) were not evaluated because they show embryonic lethality.[33] *Bdnf* gene expression in brain cortices of (Glut3$^{+/-}$) mice was significantly higher than in Glut3$^{+/+}$ mice, supporting the notion that haploinsufficiency of Glut3 in neurons is sufficient to drive changes in glucose that result in *Bdnf* upregulation (Figures 1G–1I). These data indicate that 2-DG increases *Bdnf* gene expression both *in vitro* and *in vivo*.

Since BDNF modulates long-term potentiation (LTP), a cellular and electrophysiological process relevant to learning and memory,[34] we assessed the effect of 2-DG treatment on LTP in hippocampal slices. LTP was significantly increased in response to acute treatment with 2-DG for 6 h (Figure 1J). Thus, 2-DG increases *Bdnf* gene expression *in vitro* and *in vivo* and increases LTP, a neurophysiological correlate of learning and memory, in hippocampal slices.

2-DG treatment improves functional outcomes after ischemic stroke

The dose of 2-DG (10 mg/kg) that induced *Bdnf* in the brain was two orders of magnitude less than that used in prior studies.[3,32] Prior to investigating the mechanism, we verified that 2-DG, at these low doses, had an integrated, salutary effect. Accordingly, 2-DG was administered 24 h after inducing transient middle cerebral artery occlusion (MCAO) in mice every day for 4 weeks (Figure 2A). This model was chosen because it mimics human ischemic stroke.[35] As outcomes, we assessed unilateral sensorimotor dysfunction (the corner test or tape removal test) and sensorimotor dysfunction related to striatal damage (the pole test) at distinct intervals after initiating treatment.[36,37] 2-DG treatment beginning at 24 h post-stroke led to significant behavioral recovery in all tests (Figures 2B–2D). In all cases, improvement in sensorimotor behaviors was observed 1–2 weeks following

the administration of 2-DG, suggesting a delayed effect on recovery rather than an immediate effect on neuroprotection (Figure 2G). Consistently, we found no difference in infarct size between vehicle and 2-DG-treated mice 3 days after stroke onset (Figures 2E and 2F). 2-DG injection daily for 3–4 weeks did not cause changes in physiological parameters that could affect stroke outcomes independent of BDNF (Table S1). It also did not increase levels of urinary ketones, suggesting that the effects of 2-DG at doses sufficient to induce *Bdnf* in the brain and improve functional recovery do not require systemic ketogenesis (Figures S1D and S1E).

2-DG normalizes learning and memory deficits in 5xFAD mice

Since BDNF is significantly downregulated in post-mortem AD brains[38] and driving BDNF levels up improves learning and memory deficits in preclinical models of AD,[39,40] we hypothesized that 2-DG would also improve cognitive outcomes in murine AD. Therefore, we used a 5xFAD transgenic mouse, a well-established AD model expressing human amyloid precursor protein (APP) and human presenilin 1 (PSEN1) transgenes with five AD-linked mutations. The 5xFAD mouse develops amyloid pathology beginning age 2 months[41] and shows a decline in spatial memory in the Y-maze (spontaneous alternation test) and Morris water maze at ~6 months.[42,43] Because 2-DG induced BDNF in cultured neurons, direct delivery of 2-DG to the brain might increase *Bdnf* gene expression and improve outcomes in the 5xFAD mouse (versus saline). Since the ED$_{50}$ (median effective dose value) of drugs injected through an intracerebroventricular (i.c.v.) route is usually around 10-fold less than the ED$_{50}$ of drugs injected through an i.p. route to achieve a similar effect on the brain,[44] we tested either saline alone or 2-DG dissolved in saline (1 mg/kg/day) for 4 weeks through an Alzet mini-osmotic pump (Figure 3A). *Bdnf* mRNA levels significantly increased in hippocampal slices from 5xFAD mice infused with 2-DG compared with saline alone (Figure 3B). Similarly, 4 weeks of 2-DG infusion normalized LTP to a level like that of WT mice infused with saline (Figure 3C).

In parallel, we examined changes in spatial working memory induced by chronic CNS-directed 2-DG delivery using a spontaneous alternation test in a Y-maze. 2-DG (1 mg/kg/day) resulted in a trend toward the normalization of short-term memory in 5xFAD mice (Figures 3D and 3E). Spatial long-term memory was assessed using the Morris water maze. 2-DG normalized this capacity in 5xFAD mice to a level approximating that of WT mice treated with saline (Figures 3F–3H). 2-DG showed no nootropic increase in WT mice in either the Y-maze or Morris water maze task (Figures 3D–3H). These data suggest that 2-DG improves AD-related learning and memory defects by normalizing BDNF levels (Figure 3I). The release of 2-DG through the Alzet mini-osmotic pump for 4 weeks did not increase BHB levels in the brain (Figures S1F and S1G), suggesting that the effects of low glucose are independent of ketone bodies.

Energy sensing is unnecessary for 2-DG-driven increase in *Bdnf* gene expression

The significant effect of 2-DG (at doses that induce *Bdnf*) on behavioral outcomes in models of stroke and AD motivated a
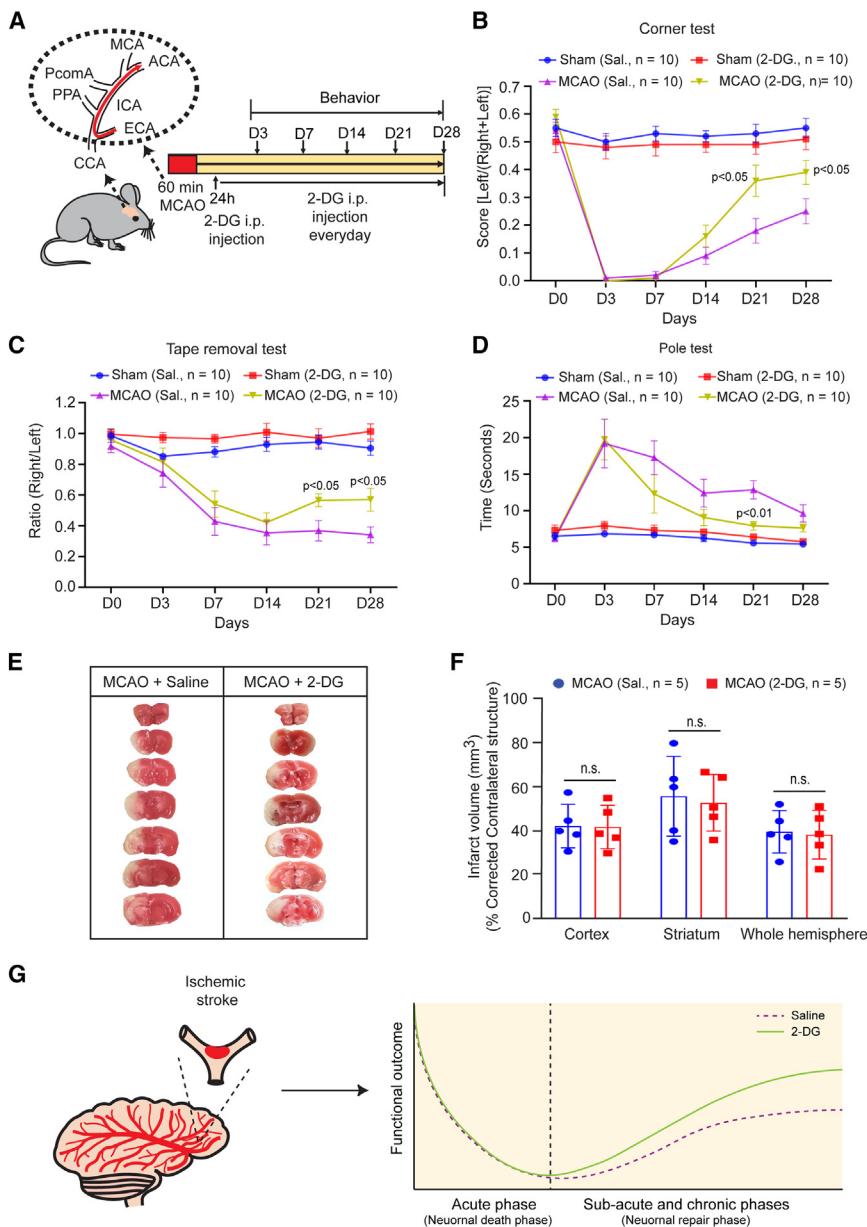
Figure 2. Post-stroke 2-DG treatment improves sensory and motor functional recovery

(A) Schematic diagram of the experimental protocol for inducing ischemic stroke. 60 min MCAO in the mouse was followed by intraperitoneal 2-DG (10 mg/kg) and behavioral assessments at various time intervals.

(B) Corner test. Two-way ANOVA with repeated measures. For statistical details, see Table S2.

(C) Tape removal test. Two-way ANOVA with repeated measures. For statistical details, see Table S2.

(D) Pole test. Two-way ANOVA with repeated measures. For statistical details, see Table S2.

(E and F) Infarct size at day 3 following MCAO. Following MCAO, mice were injected with either saline or 2-DG (10 mg/kg) i.p. at 24 and 48 h and 2,3,5-triphenyltetrazolium chloride (TTC) staining was done at 72 h (mean ± SEM, two-way ANOVA with Šidák's multiple comparison test).

(G) Schematic of 2-DG's effects on behavior when delivered 24 h following stroke.

AMPK phosphorylation mediates *Bdnf* upregulation, we inhibited AMPKα1 phosphorylation using a dominant-negative AMPKα1 (Figures 4F and 4G). Reducing AMPKα1 phosphorylation did not abrogate the 2-DG-stimulated increase in *Bdnf* message (Figure 4H). Thus, an increase in *Bdnf* message may not result from 2-DG-induced AMPK activation (Figure 4I).

2-DG-driven increases in *Bdnf* gene expression and LTP are dependent on transcription showing a dominant ER stress-associated gene signature

Glucose is a key molecule in transcriptional processes.[46,47] We tested whether 2-DG-induced increases in *Bdnf* message and LTP are transcription-dependent by co-treating primary neurons or

search for the mechanism by which 2-DG increases BDNF. 2-DG affects energy production by inhibiting glycolytic metabolism, thus reducing pyruvate transport into the mitochondria and ATP generation. As predicted, 2-DG (10 mM) increased the AMP-ATP ratio, as measured by laser capture mass spectrometry (Figure 4A) in cortical neurons. Accordingly, energy sensing could mediate crosstalk between 2-DG-driven metabolic signaling and transcriptional changes in the *Bdnf* gene. AMP kinase (AMPK) is considered a bioenergetic sensor that responds to increased AMP and decreased ATP levels by increasing phosphorylation at threonine 172 of its α1 subunit.[45] Primary neurons treated with increasing concentrations of 2-DG (1–15 mM) exhibited a weak correlation between the level of AMPKα1 activation and *Bdnf* expression (Figures 4B–4E). To determine whether

hippocampal slices with 2-DG and a transcriptional inhibitor, actinomycin D (ActD, 1–2 μg/mL). This concentration of ActD inhibits global transcription in cortical neurons.[48] Inhibiting transcription with ActD completely blocked the ability of 2-DG to increase *Bdnf* message in cortical cultures and hippocampal slices (Figures 5A and 5B). Similarly, ActD completely blocked the 2-DG-mediated induction of LTP (Figure 5C). Therefore, the inductions of *Bdnf* message and LTP by 2-DG are likely transcription-dependent (Figure 5D).

The transcription dependence of 2-DG's effects prompted examination of the transcriptome following 2-DG treatment. We used an unbiased RNA sequencing (RNA-seq) approach with two aims: (1) to investigate whether 2-DG treatment leads to changes in other genes involved in plasticity, learning, or
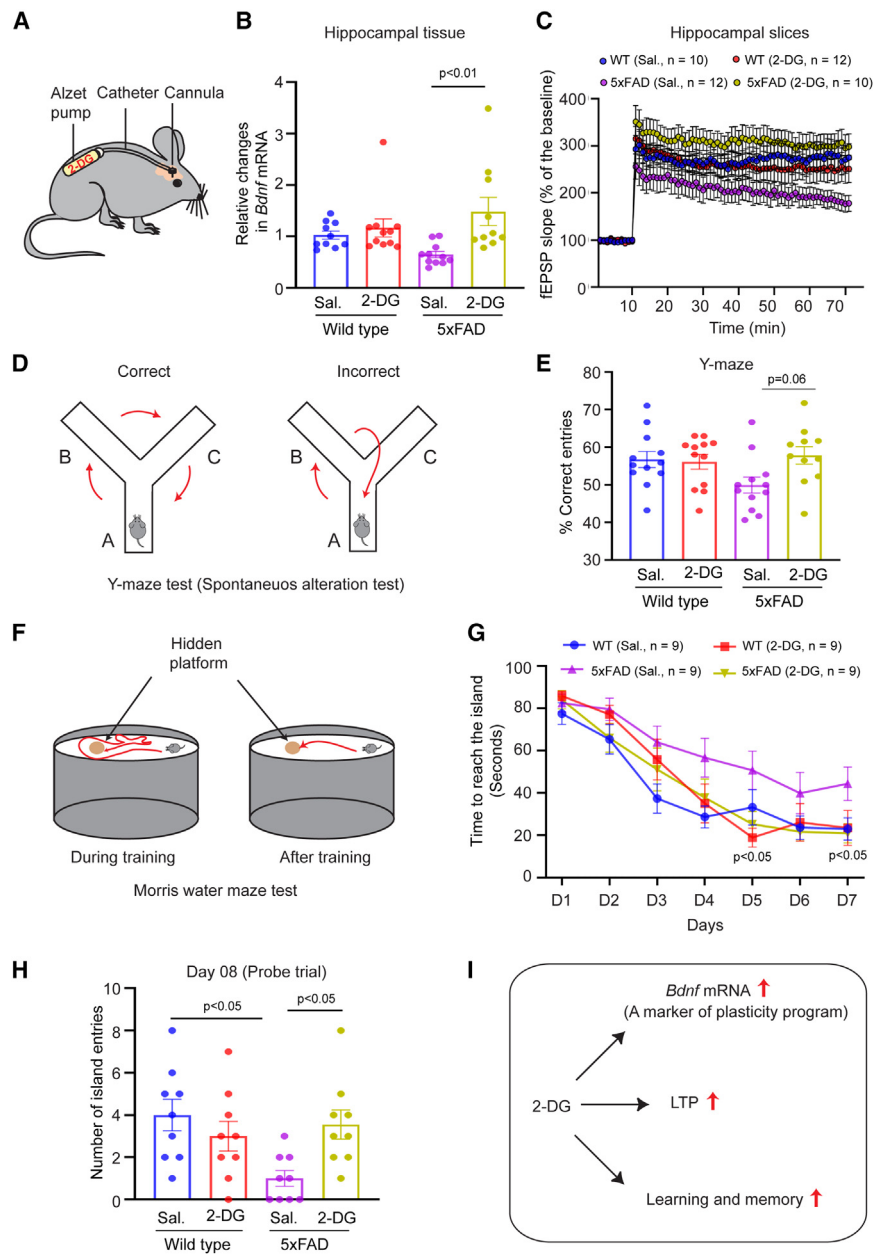
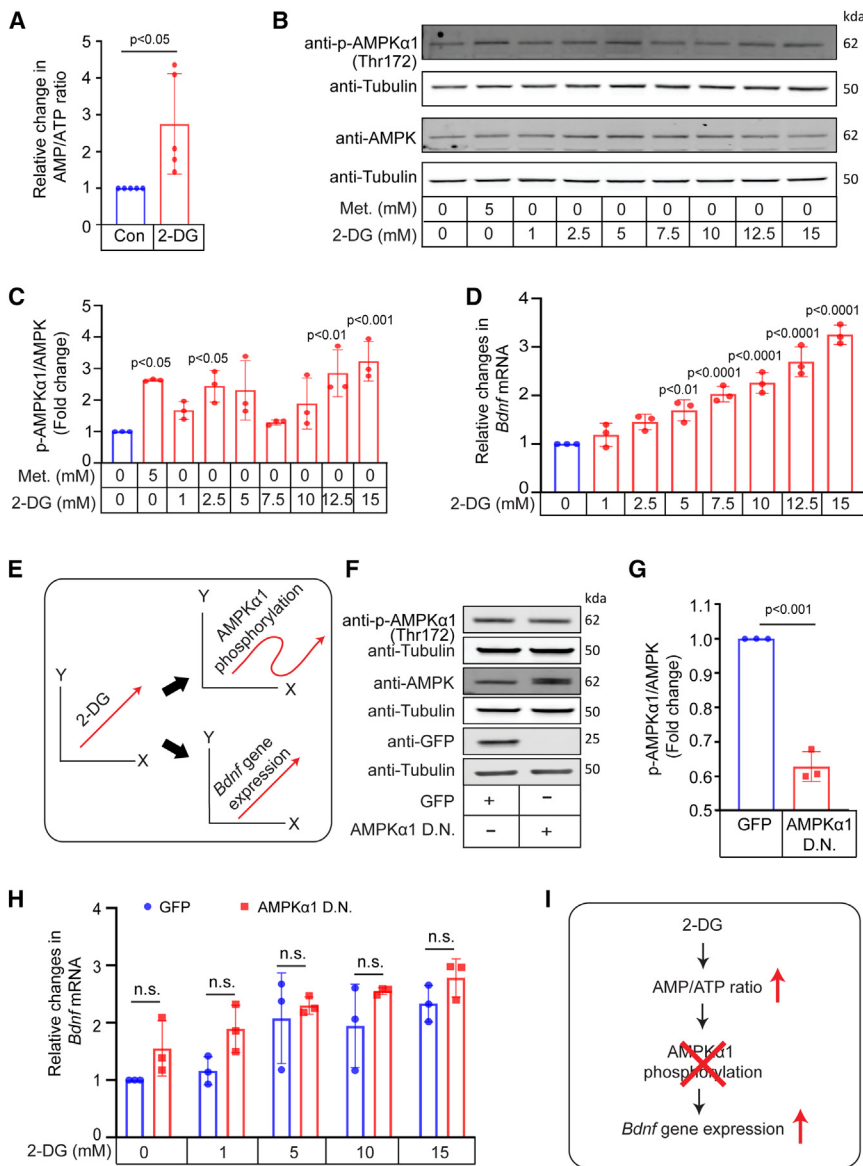**Figure 3. 2-DG normalizes learning and memory deficit in 5xFAD mice**

(A) Schematic diagram of experimental paradigm. Alzet (osmotic) pumps filled with either saline or 2-DG implanted below the neck of 6-month-old wild-type or 5xFAD mice and connected with its catheter tube to the brain cortex through i.c.v. injection, allowing the slow release of either saline or 2-DG for 4 weeks.

(B) Messenger RNA levels of *Bdnf* from brain hippocampi (two-way ANOVA with Turkey's multiple comparison test).

(C) Levels of LTP elicited by 3 × theta-bursts in hippocampal slices.

(D) Schematic diagram of spontaneous alternation (Y-maze) behavior analysis.

(E) Spontaneous alternation behavior (two-way ANOVA with Turkey's multiple comparison test).

(F) Schematic diagram of Morris water maze behavioral outcomes.

(G) Data from 7-day spatial reference memory training to reach the island (hidden platform).

(H) The probe trial of the wild-type and 5xFAD mice on day 8 (two-way ANOVA with Turkey's multiple comparison test).

(I) Summary showing that 2-DG significantly induces Bdnf, enhances LTP, and restores memory in 5xFAD mice.

***Statistical details for all figures can be found in Table S2.

memory and (2) to find the most dominant gene signatures in response to 2-DG treatment. Analysis confirmed an increase in the expression of *Bdnf* at 1 mM 2-DG and, consistent with our qPCR results (Figure 1), an even larger increase at 10 mM 2-DG (Figure 5E). Other genes implicated in plasticity, learning, and memory were upregulated, including *Creb1*, *CaM kinase IID* and *IIG*, *ryanodine receptor 2* (*Ryr2*), *Xpo4*, *Pten*, *Xbp1*, and *Atf4*. We focused on Xbp1 and ATF4, as these transcription factors (TFs) are both associated with *Bdnf* or plasticity gene expression[49,50] and induced by ER stress. Gene set enrichment analysis (GSEA) showed maximal upregulation of the gene signatures related to ER stress in response to 2-DG treatment (Figures 5F and S2A). Moreover, cellular

component enrichment analysis showed significant enrichment of genes related to the ER (Figures 5G and S2B), indicating that ER is a crucial organelle affected by 2-DG treatment. All genes related to ER stress showed a concentration-dependent increase in response to 1 and 10 mM concentrations of 2-DG (Figure 5H).

The ER is involved in protein homeostasis by ensuring the proper folding of proteins with the help of chaperones, including GRP78 (glucose regulated protein 78), also known as Bip or HSPa5. Glucose plays a vital role within the ER by contributing through nicotinamide adenine dinucleotide phosphate (NADPH) production or N-linked glycosylation. Agents that diminish glucose utilization, such as 2-DG, can activate ER stress, an adaptive response that triggers downstream signaling cascades, leading to restoration of protein homeostasis. To test whether 2-DG enhances the phosphorylation of eIF2α, a convergent signaling molecule in the ER stress response, we performed immunoblotting using a serine 51 phosphospecific antibody. 2-DG increased eIF2α phosphorylation (Figures 5I and 5J). eIF2α serine 51 phosphorylation sequesters the guanine nucleotide exchange factor and decreases translational initiation to reduce the number of client proteins in the ER by reducing the ternary initiation complex. Simultaneously, rate-limiting amounts of the ternary complex

Figure 4. 2-DG-mediated induction of *Bdnf* message does not require AMPK energy sensing

(A) AMP/ATP ratio calculated from peak intensities obtained from targeted metabolic profiling the study of mouse primary neurons (mean ± SD, Student's t test).

(B and C) 2-DG treatment for 4 h in mouse neurons. Metformin (Met. 5 mM), an AMP kinase activator, was used as a positive control (mean ± SD, one-way ANOVA with Dunnett post hoc test).

(D) 2-DG treatment for 6 h in mouse primary neurons (mean ± SD, one-way ANOVA with Dunnett post test).

(E) Schematic diagram of the dissociation between p-AMPKα1 phosphorylation and *Bdnf* gene expression.

(F and G) Reduced AMPKα1 phosphorylation following overexpression of dominant-negative AMPK (mean ± SD, Student's t test).

(H) 2-DG treatment for 6 h in mouse neurons overexpressing GFP or dominant-negative AMPKα1 (AMPKα1 D.N.) for 48 h (mean ± SD, two-way ANOVA with Šidák's multiple comparisons test).

(I) Schematic summary showing that the 2-DG-led increase in plasticity is not mediated by AMPKα1 phosphorylation.

2-DG-led increases in *Bdnf* gene expression and LTP are dependent on transcription that shows a dominant ER stress-associated gene signature (Figure 5M).
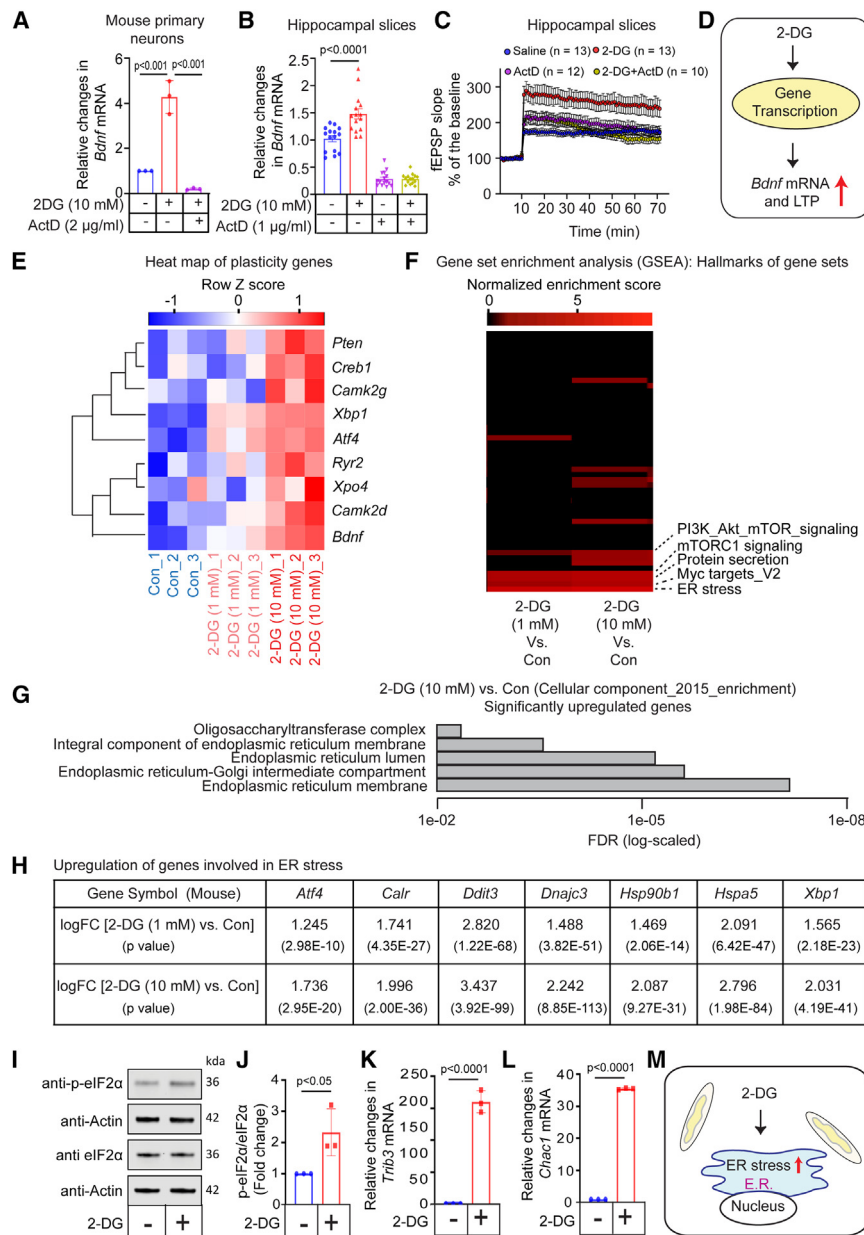
2-DG decreases glucose and mannose availability, which reduces N-linked glycosylation, induces sublethal ER stress, and drives *Bdnf* expression via ATF4

Cell enrichment compartment analysis also revealed genes in the oligosaccharide-transferase complex as significantly regulated by 2-DG. This complex transfers 14 component sugars composed of glucose and mannose from dolichol to nascent chain asparagines to complete N-linked glycosylation, which is essential for folding secreted and plasma membrane-linked proteins and mediated through glucose- and mannose-derived glycans.[53] These post-translational modifications occur as proteins (40%–60% of proteins, depending on the cell type) are translated into the ER.

To evaluate whether diminished N-linked glycosylation leading to ER stress activation mediates 2-DG-induced transcriptional upregulation of the *Bdnf* gene, we assessed whether the addition of glucose or mannose to the media of primary neurons could reverse 2-DG-driven *Bdnf* gene expression. Indeed, increasing concentrations of glucose or mannose decreased 2-DG-induced *Bdnf* message in a concentration-dependent manner, consistent with the hypothesis that 2-DG-diminished N-linked glycosylation drives the 2-DG-induced *Bdnf* message

paradoxically translate mRNAs, such as ATF4, that contain upstream open reading frames (uORFs) upstream of the ATF4 open reading frame (ORF). ATF4 is a TF that both enhances the transcription of genes involved in compensation to ER stress and regulates the expression of genes involved in plasticity, LTP, learning, and memory.[50] Thus, it emerged as the primary candidate to drive ER stress and *Bdnf* expression. Ingenuity pathway analysis for upstream transcriptional regulators showed a significant upregulation of a broad cassette of ATF4 target genes in response to 2-DG treatment (Fisher's exact test, p < 0.05, Figure S2C). We verified that known ATF4 target genes, Tribbles 3 (*Trib3*), a modulator of AKT, and *Chac1*, a cyclohydrolase that degrades glutathione,[51,52] were induced by 2-DG (Figures 5K and 5L). Reducing glucose in the media also drove the expression of *Trib3* and *Chac1* (Figures S4B, S4C, S4H, and S4I). These data suggest that

Figure 5. 2-DG-mediated effects are associated with a significant ER stress gene signature

(A) 6 h treatment of 2-DG in the absence or presence of the transcriptional inhibitor, actinomycin D (ActD) in mouse neurons (mean ± SD, one-way ANOVA with Bonferroni post hoc test).

(B) Hippocampal slices were submerged in artificial cerebrospinal fluid (ACSF) with either saline, 2-DG, or 2-DG plus ActD for 6 h (mean ± SEM, one-way ANOVA with Bonferroni post hoc test).

(C) LTP measurements from hippocampal slices were submerged in ACSF with vehicle, 2-DG (10 mM), ActD (1 μg/mL), or 2-DG plus ActD for 6 h. For statistical details, see Table S2.

(D) Schematic summary of transcription dependence of 2-DG-induced increases in *Bdnf* message and LTP.

(E) A heatmap showing concentration-dependent changes in scaled expression of genes associated with 2-DG treatments for 6 h in mouse neurons.

(F) GSEA indicating changes in hallmarks of gene sets with 2-DG treatments for 6 h in mouse primary neurons. Values are normalized enrichment scores.

(G) Cellular component gene ontology (GO) analysis. The FDR (false discovery rate) values are indicated in log scale.

(H) The differential expression of genes related to ER stress with 2-DG treatments for 6 h.

(I and J) 2-DG (10 mM) treatment for 2 h in mouse primary neurons (n = 3, mean ± SD).

(K and L) 2-DG treatment for 6 h in mouse primary neurons (mean ± SD, Student's t test).

(M) Schematic summary showing that ER stress is the dominant effector of 2-DG-induced RNA changes.

diminishing global translational initiation but enhancing translation of the transcription factor, ATF4. To evaluate whether PERK, eIF2α, and ATF4 are necessary for the 2-DG-driven upregulation of the *Bdnf* message, we treated primary neurons with GSK2606414, a selective PERK inhibitor[56] that blocks PERK-induced eIF2α phosphorylation. GSK2606414 significantly inhibited 2-DG-induced eIF2α phosphorylation (Figures 6G and 6H) and transcription of the ATF4 target gene, *Trib3*, in primary neurons[51] (Figures 6I and 6J). In parallel, the same concentration of GSK2606414 blocked 2-DG's ability to induce expression of *Bdnf* (Figure 6K). GSK2606414 completely blocked both the expression of *Trib3* and *Chac1* in response to low extracellular glucose and its ability to drive *Bdnf* gene expression (Figures S4D–S4F and S4J–S4L). Thus, the PERK-eIF2α-ATF4 axis is induced by 2-DG or low glucose, and these events culminate in increased *Bdnf* expression in primary neurons.

To test whether eIF2α phosphorylation is sufficient to increase *Bdnf* message and upregulate LTP, we conditionally deleted protein phosphatase 1 (pp1) regulatory subunit 15 (Ppp1R15).
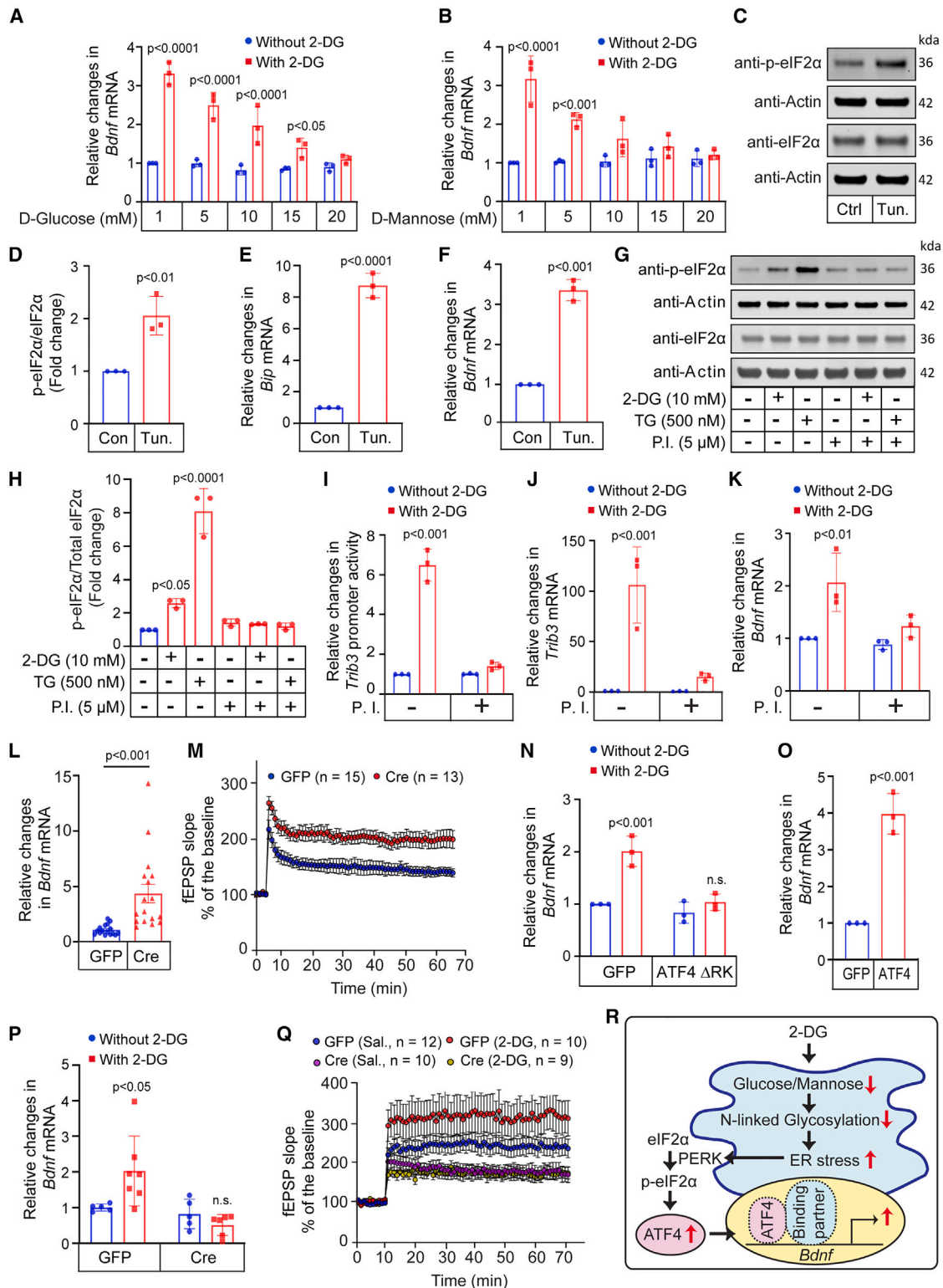
(Figures 6A and 6B). Next, we examined whether inhibition of N-linked glycosylation was sufficient to upregulate *Bdnf* expression. We treated primary neurons with tunicamycin, a pharmacological inhibitor of N-linked glycosylation,[54] for 6 h, which has also been shown to drive ER stress.[55] Tunicamycin induced an expected increase in the phosphorylation of eIF2α (Figures 6C and 6D) and an increased expression of the ER stress chaperone *Bip* (Figure 6E). The same concentration of tunicamycin led to a significant increase in the expression of *Bdnf* (Figure 6F), indicating that inhibition of N-linked glycosylation appears necessary and sufficient to induce *Bdnf* message.

Diminished N-linked glycosylation leads to the release of Bip and the disinhibition of transmembrane protein kinase RNA-activated (PKR)-like ER kinase (PERK). PERK phosphorylates eIF2α,

Figure 6. ATF4 mediates the 2-DG induction of *Bdnf* expression

(A and B) 6 h treatments in mouse neurons (mean ± SD, two-way ANOVA with Bonferroni post hoc test).

(C and D) Tunicamycin (3 μM), an inhibitor of N-linked glycosylation, for 2 h in mouse neurons (mean ± SD, Student's t test).

(E and F) Tunicamycin (3 μM) treatment for 6 h in mouse primary neurons (mean ± SD, Student's t test).

(legend continued on next page)

Together with pp1, Ppp1R15 specifically catalyzes the dephosphorylation of eIF2α. Conditional deletion of this phosphatase leads to constitutive phosphorylation of eIF2α.[57] Ppp1r15b was deleted in the hippocampus of the Ppp1r15b^{fl/fl} mouse by intracranial injection of AAV8-Cre. We verified the activation of eIF2α phosphorylation by examining the activation of downstream ATF4 target genes, such as *Trib3*, *Chac1*, and *Ddit3*, in the hippocampus (Figures S3A–S3C). Activation of eIF2α phosphorylation led to a significant increase in *Bdnf* gene expression in the hippocampus (Figure 6L) with a significant increase in LTP (Figure 6M). eIF2α phosphorylation is, therefore, sufficient for inducing both *Bdnf* gene expression and LTP.

Because 2-DG-induced *Bdnf* gene expression and LTP are transcription-dependent (Figures 5A–5D) and 2-DG leads to an upregulation of an array of ATF4 target genes (Figure S2C), we hypothesized that the 2-DG-induced increase in *Bdnf* expression is mediated by ATF4 transcriptional activation. To test whether 2-DG requires an ATF4 binding site to drive the expression of one of its target genes, *Trib3*, we expressed *Trib3* promoter reporter plasmids without or with a 33 base-pair ATF4 binding site (i.e., Trib3 WT and Trib3Δ33bp).[51,58] As predicted, the ATF4 binding site mutant completely blocked the 2-DG-driven induction of *Trib3* promoter activity (Figure S3F).

We examined whether ATF4 activity was necessary for increases in the *Bdnf* mRNA message. We inhibited ATF4 activity via viral-mediated expression of dominant-negative ATF4 (ATF4ΔRK, which lacks the ATF4 DNA binding domain) in primary neurons. ATF4 inhibition blocked 2-DG's ability to drive *Bdnf* message levels (Figure 6N). We then assessed whether ATF4 was sufficient for upregulating the *Bdnf* message. We forced the expression of WT ATF4 in primary neurons for 24 h. ATF4 was sufficient to drive expression of ER stress-associated genes, *Chac1* and *Trib3*, but also *Bdnf* in primary neurons (Figures 6O and S3D–S3E).

To determine whether 2-DG-driven hippocampal ATF4 expression is required to drive *Bdnf* gene expression and synaptic plasticity *in vivo*, we conditionally deleted ATF4 in the CA1 and CA3 regions of each adult hippocampus in ATF4^{fl/fl} mice using AAV9 (Figure S3G). 2-DG-driven *Bdnf* gene expression and LTP were reduced in hippocampal slices (Figures 6P and 6Q) with decreased expression of ATF4. Our results suggest that 2-DG reduces N-linked glycosylation, induces sublethal ER stress, and drives *Bdnf* expression and LTP via hippocampal ATF4 *in vivo* (Figure 6R).

ATF4 directly regulates transcription of the *Bdnf* gene

We sought to determine whether ATF4, a known transcriptional activator, directly binds to the *Bdnf* promoter to increase *Bdnf* gene expression in response to 2-DG treatment. We performed a chromatin immunoprecipitation sequencing (ChIP-seq) experiment using a specific antibody against ATF4 in primary neurons treated with 2-DG for 6 h.[52] 2-DG did not induce an increase in ATF4 binding at the promoter region upstream of the TSS (transcription start site). Instead, ATF4 was selectively enriched (indicated by a single ChIP-seq peak in the University of California Santa Cruz (UCSC) genome browser in the 2-DG treated i.p. fraction) near a 3 kb intron region downstream of the *Bdnf* exon I TSS (Figure 7A). This +3 kb intron region with a single ATF4 ChIP-seq peak corresponds precisely with the +3 kb region previously identified as a region capable of regulating *Bdnf* gene expression as an enhancer.[59] This ATF4 binding enhancer is evolutionarily conserved among mammals, further suggesting its importance in *Bdnf* gene regulation (Figure S5).

As enhancer regions can drive the transcription of enhancer RNA (eRNA),[59] we first sought to confirm the enhancer function of the +3 kb intron sequence with a single ATF4 ChIP-seq peak by asking whether 2-DG drives the transcription of +3 kb eRNA. The RNA-seq data showed a significant increase as a function of 2-DG concentration in the expression of +3 kb eRNA (Figure 7B). A similar result was obtained with quantitative real-time PCR, which indicated a significant increase in antisense eRNA expression in response to 2-DG treatment in primary neurons (Figure 7C).

Since *in vitro* data in primary neurons suggested that 2-DG induced +3 kb eRNA expression (Figures 7B and 7C) by driving specific binding of ATF4 to this site (confirmed by ChIP-seq analysis, Figure 7A), we sought *in vivo* evidence that ATF4 activation is sufficient to induce +3 kb eRNA expression. We examined RNA from the hippocampus of Ppp1r15b^{fl/fl} mice. Conditional deletion of Ppp1r15b in the hippocampus led to a constitutive phosphorylation of eIF2α and downstream activation of ATF4 signaling as confirmed by significant upregulation of canonical ATF4 target genes *Trib3*, *Chac1*, and *Ddit3* (Figures S3A–S3C). Upregulation of *Bdnf* gene expression and improvement in LTP were observed (Figures 6L and 6M). Moreover, upregulation of eRNA expression (Figure 7D) suggests that ATF4 activation is sufficient to drive BDNF-associated +3 kb enhancer activity in the hippocampus.

We determined whether the transcriptional activity of ATF4 is necessary to drive recruitment of RNA polymerase II (RNA

(G and H) The co-treatment of PERK inhibitor I (GSK2606414) with 2-DG or thapsigargin (a positive control for ER stress) for 2 h in mouse primary neurons (mean ± SD).

(I) The co-treatment of PERK inhibitor I (5 μM) with 2-DG (10 mM) for 9 h (mean ± SD, two-way ANOVA with Bonferroni post hoc test).

(J and K) The co-treatment of PERK inhibitor I (5 μM) with 2-DG (10 mM) for 6 h (mean ± SD, two-way ANOVA with Bonferroni post hoc test).

(L and M) Changes in levels of *Bdnf* mRNA and LTP, respectively, in hippocampal slices from the homozygous floxed Ppp1r15b mice. Deletion was performed *in vivo* using AAV8-Cre double injection in each hippocampus. AAV8-GFP was injected as a viral control.

(N) 2-DG treatment for 6 h in neurons transiently overexpressing GFP or dominant-negative ATF4 for 48 h as described[51] (mean ± SD, two-way ANOVA with Bonferroni post hoc test).

(O) Adenoviral constructs encoding ATF4 or GFP were used to force expression of their respective cargoes for 24 h (mean ± SD, Student's t test).

(P and Q) Changes in *Bdnf* mRNA levels and LTP, respectively, in hippocampal slices from the ATF4^{fl/fl} mice with and without Cre-mediated reduction of neuronal ATF4 in their hippocampi. Hippocampal slices were submerged either in ACSF (vehicle) alone or ACSF with 10 mM 2-DG for 6 h. For statistical details, see Table S2.

(R) Schematic diagram of events downstream of 2-DG that led to ER stress-induced eIF2α phosphorylation, the paradoxical translation of ATF4, and the induction of BDNF (and other plasticity genes).
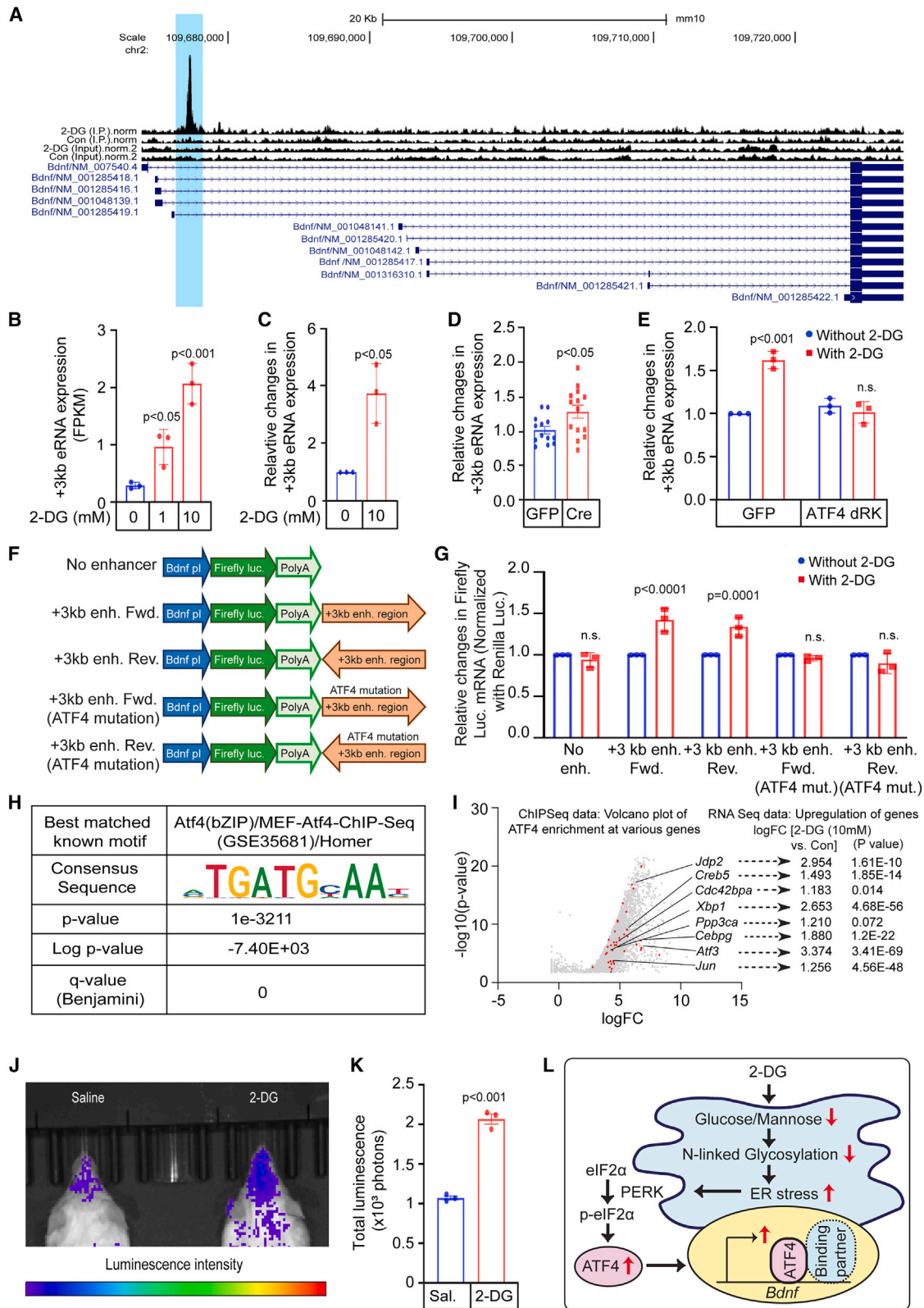
(legend on next page)

Pol II) to the +3 kb enhancer and induce *Bdnf* gene expression in response to 2-DG. To do this, we evaluated if ATF4ΔRK (ATF4 DNA binding site mutation), which blocks 2-DG mediated induction of *Bdnf* message, could also block 2-DG-induced eRNA expression. ATF4ΔRK (ATF4 DNA binding site mutation) completely blocked 2-DG-driven eRNA expression (Figure 7E). 2-DG-driven eRNA expression was also reduced in hippocampal slices with conditional deletion of neuronal ATF4, indicating that neuronal ATF4 drives 2-DG-induced eRNA expression (Figures S3G and S3H).

We next examined whether ATF4 binding to the +3 kb enhancer region (Figure 7A) is critical for 2-DG-induced *Bdnf* gene expression. Accordingly, we used a *Bdnf* promoter-driven luciferase expression cassette with the +3 kb enhancer region sequence (in forward or reverse orientation to the rat *Bdnf* gene) cloned downstream. We also mutated the ATF4 binding sequence (tgatgcaa to ggatgacc) within this +3 kb enhancer region (Figure 7F). 2-DG led to increases in reporter expression in primary neurons expressing a *Bdnf* promoter I firefly luciferase construct containing a +3 kb forward or reverse enhancer. Mutation of the ATF4 binding site in the +3 kb enhancer region (corresponding to the site of enrichment of ATF4 binding by ChIP) blocked 2-DG-induced increases in reporter expression (Figure 7G). Thus, specific ATF4 binding to the +3 kb enhancer region is necessary for increases in *Bdnf* gene expression-induced 2-DG. Indeed, ChIP-seq data showed that 2-DG increased the binding of ATF4 to regulatory regions of other known plasticity genes. Specifically, 2-DG treatment enhanced binding of ATF4 to the regulatory regions of *Jdp2*, *Creb5*, *Cdc42bpa*, *Xbp1*, *Ppp3ca*, *Cebpγ*, *Atf3*, and *Jun*. Of note, these genes were also upregulated in our RNA-seq analysis, supporting the notion that ATF4 drives the upregulation of a cassette of genes associated with plasticity in response to 2-DG (Figure 7I).

To further investigate the transcriptional role of ATF4, we probed motif occurrence from the ATF4 binding sites identified by ChIP-seq using *de novo* motif analysis.[60] The ATF4 motif was identified as the most enriched motif that overlaps within the ChIP-seq peak of the +3 kb intron region (Figure 7H). ATF4

is a basic leucine zipper domain (bZIP) family TF that homodimerizes or heterodimerizes to affect target genes.[61] *De novo* motif analysis returned enriched sequences of TFs such as CHOP, CEBP:AP1, CEBPα, DDIT3:CEBPα, CEBPβ, JUN, and JUN(Var.2) within the peak region (Figure S6). Among these candidates, previous studies found enrichment of TFs such as CEBPγ, CEBPβ, and JUND in the +3 kb region.[59,62,63]

Our findings suggest that 2-DG-induced activation of ER stress leads to enhanced translation of ATF4, which transcriptionally regulates *Bdnf* gene expression. This model predicts that in response to 2-DG, paradoxical translation via the 5' UTR containing two uORFs and the ORF of ATF4 fused to luciferase as a reporter for ATF4 should occur *in vivo*. We overexpressed 5' UTR ATF4 luciferase reporter using an AAV8 viral vector in the CD1 mouse brain for 3 weeks and then injected 2-DG (i.c.v.) for 4 h. We found an increase in ATF4 reporter translation in the brain, as monitored by *in vivo* bioluminescence imaging (Figures 7J and 7K). Since IVIS imaging is a two-dimensional image of three-dimensional tissue, we confirmed that increases in ATF4 reporter activity in cortical lysates from these mice (Figure S7). We conclude that 2-DG-induced activation of ER stress leads to enhanced translation of ATF4, which regulates *Bdnf* and other plasticity genes.

These data establish that 2-DG regulates the expression of *Bdnf* and other "plasticity-associated" genes. 2-DG does so via an adaptive, sublethal ER stress response involving reductions in N-linked glycosylation. This response culminates in ATF4 binding to its response element in the +3 kb intronic enhancer region of *Bdnf* (Figure 7L). N-linked glycosylation is a sensitive indicator of 2-DG modifications in glucose metabolism.

DISCUSSION

IF is a nutritional paradigm gaining acceptance as a lifestyle choice worldwide. This acceptance has been catalyzed by clarifying the molecular mechanisms by which IF augments organ health, particularly the brain.[13] Attention has been focused on the metabolic switch from low glucose to ketone body utilization

---

Figure 7. ATF4 binds the *Bdnf* gene at an intronic region +3 kb from the transcriptional start site and regulates Bdnf gene expression

(A) A UCSC Genome Browser view of the representative ChIP-seq showing ATF4 enrichment at an intronic region 3 kb downstream of *Bdnf* exon I TSS with 2-DG treatment (10 mM) for 6 h in mouse neurons (n = 5, mean ± SD).

(B) Changes in RNA-seq FPKM values (fragments per kilobase of transcript per million mapped fragments) for +3 kb enhancer RNA (eRNA) with 6 h treatment of 2-DG in mouse primary neurons (mean ± SD, one-way ANOVA with Dunnett post hoc test).

(C) Real-time PCR data confirming changes in +3 kb eRNA expression with 2-DG treatment for 6 h in mouse primary neurons (mean ± SD, Student's t test).

(D) +3 kb (eRNA) levels in hippocampal slices from the Ppp1r15b^{fl/fl} mice (mean ± SEM, Student's t test)

(E) 2-DG treatment for 6 h following forced expression of GFP or dominant-negative ATF4 in mouse neurons (mean ± SD, two-way ANOVA with Tukey's multiple comparisons test).

(F) Schematic diagram of luciferase reporter constructs utilized to study BDNF regulation.

(G) 10 mM 2-DG treatment for 6 h in primary neurons (*Firefly luciferase* ct values were normalized with corresponding *Renilla luciferase* ct values) (mean ± SD, two-way ANOVA with Šidák's multiple comparisons test).

(H) *De novo* motif analysis of the ATF4 differential binding peaks showed a canonical ATF4 binding site as the most enriched motif sequence within the peak region (n = 5, mean ± SD).

(I) A volcano plot of differential peak calls of various genes (plasticity genes indicated in red) induced by 10 mM 2-DG treatment for 6 h in primary neurons. Data were analyzed using DiffBind (DESeq2) (n = 5, mean ± SD).

(J and K) *In vivo* bioluminescence imaging of paradoxical translation of an ATF4 reporter by 2-DG (25 μg 2-DG, 1 mg/kg i.c.v.) treated mouse (4 h) (Student's t test, mean ± SD).

(L) Schematic diagram of the 2-DG-led upregulation of *Bdnf* gene expression through direct binding of ATF4 to the *Bdnf gene regulatory region*. We speculate that homodimerization with ATF4 itself or heterodimerization with other potential binding partners may be key, as shown in Figure S6.

and how it drives signaling to enhance the expression of resilience genes, including survival, growth, and plasticity factors such as BDNF. Here, we used 2-DG to suggest a novel mechanism by which one component of IF, glucose restriction, induces BDNF and other plasticity and resilience genes. Rather than ketosis, we used the upregulation of *Bdnf* as a molecular target for 2-DG dosing. We were able to demonstrate (1) significant therapeutic effects on learning and memory deficits in an AD mouse model and (2) enhanced sensorimotor recovery following ischemic stroke (Figures 2 and 3). In prior hippocampal studies of BDNF induction, rats were injected i.p. with 250 mg/kg/day 2-DG for 2 weeks. By contrast, we found changes in *Bdnf* expression at much lower 2-DG doses than previously evaluated.[64] Accordingly, to achieve therapeutic benefit, the dosage of 2-DG used in our study (10 mg/kg) was one-two magnitudes less than in prior studies where ketosis was induced.[3,25,32] In one study, higher doses induced lethality in males, something not observed with doses here.

Studies have shown that high doses of 2-DG induce BHB, an abundant ketone, to inhibit HDAC2 or HDAC3 at the BDNF promoter.[18] We found 2-DG could drive the transcription of *Bdnf* and other genes associated with plasticity or regeneration (e.g., *Atf3*, *Cdc42bpa*, *Ppp3cc*, *Cebpγ*) independent of ketones (Figures 1A, 3B, and 5E). Additionally, 2-DG-induced changes in *Bdnf* were not mediated via homeostatic activation of AMPK in response to decreases in ATP (Figure 4H) but rather via adaptive transcription in response to diminished N-glycosylation and ER stress (Figures 5 and 6). 2-DG has been shown to inhibit glucose uptake and glycolytic metabolism via non-competitive and competitive inhibition of hexokinase and phosphoglucose isomerase, respectively,[20–23] and to compete with mannose in adding critical N-linked sugars to proteins.[65] In this scheme, 2-DG is converted to guanosine diphosphate (GDP)-2-DG and incorporated into lipid-linked oligosaccharide precursors. The extension of the formed intermediates cannot occur via the addition of mannosyl residues. Accordingly, the formation of N-linked glycoproteins is disrupted. Incomplete N-glycosylation causes accumulation of misfolded proteins and activation of the ER stress response, which is a component of the integrated stress response. As over 50% of proteins are N-glycosylated, even small changes in glucose availability via 2-DG lead to ER stress. Indeed, fasting that leads to diminished blood glucose levels also induces ER stress.[66,67]

2-DG drove *Bdnf* gene expression by increasing its transcription (Figure 5). Several TFs are activated via distinct mechanisms due to ER stress, including Xbp1, ATF6, and ATF4. Xbp1 can bind to the promoter of *Bdnf* and activate its transcription to enhance learning- and memory-related gene expression independent of its ER stress activation.[49] Here, we provide evidence supporting a model in which the leucine zipper TF, *ATF4*, downstream of 2-DG treatment and consequent of ER stress can augment *Bdnf* transcription, LTP, and behavioral improvements in two disease models. ATF4 is paradoxically translated due to eIF2α phosphorylation. We used *in vivo* bioluminescence imaging of an ATF4 5′ UTR-luciferase construct to confirm that 2-DG enhances the paradoxical translation of ATF4 in the brain (Figures 7J and 7K).[68] ATF4 transcriptionally upregulates a cassette of genes involved in adaptation to ER stress, including

amino acids and lipid biosynthesis. We found that it can also drive *Bdnf* transcription. While studies in Aplysia and mice indicate ATF4 is a transcriptional suppressor of cAMP response element binding protein (CREB)-driven memory enhancement,[69,70] others highlight the role ATF4 can play as a transcriptional activator and enhancer of plasticity.[50] Our results reinforce the positive role that ATF4 can play in mediating learning and memory, particularly in a disease-related context.

Previous studies have demonstrated that eIF2α phosphorylation can function as a rheostat for learning and memory.[71–74] Our findings can be reconciled by the intermittent nature of 2-DG-driven changes in *Bdnf* expression. During 2-DG treatment, glycosylation is reduced, ER stress is activated, and resilience and plasticity genes are transcriptionally induced. During refeeding or the metabolism of 2-DG in the body, ER stress diminishes, translation of the enhanced mRNAs occurs, and cognition and health improve. Future studies should involve experiments to test this model. This study provides a firm molecular mechanism by which fasting-mediated hypoglycemia, and 2-DG, might induce adaptive changes in genes known to enhance plasticity and resilience. They may also represent evolutionary selection in humans for activation of a pathway that allowed increased cognition in the search for food during starvation.[13]

The prospect of using 2-DG as a therapeutic drug in AD or stroke patients in the clinical setting seems propitious. It crosses the blood-brain barrier, as indicated by radiologic studies. Moreover, safe doses of 2-DG as an anticancer agent have been assessed through a phase I/II clinical trial.[75,76] Additionally, the respective equivalent doses in humans would be around 1 mg/kg or 100 μg/kg/day,[77] much lower than the recommended safe doses of 2-DG.[75,76] Although the efficacy of 2-DG for improvement in cognitive decline in AD patients requires identification of a biomarker for target engagement and a proper clinical study, doses of 2-DG extrapolated from our animal studies are approximately 60 times lower than those used in cancer patients.

In conclusion, 2-DG could be mimetic of one aspect of IF, glucose restriction, and could drive a homeostatic response to ER stress that upregulates a host of genes involved in protein folding, protein degradation, and translational control and genes, such as *Bdnf*, implicated in plasticity. The breadth of genes positively affected by 2-DG likely explains its ability to significantly improve cognitive dysfunction in an AD model and functional recovery following ischemic stroke.

STAR★METHODS

Detailed methods are provided in the online version of this paper and include the following:

- KEY RESOURCES TABLE
- RESOURCE AVAILABILITY
  - Lead contact
  - Materials availability
  - Data and code availability
- EXPERIMENTAL MODEL DETAILS
  - Breeding and genotyping
  - Mouse primary immature cortical neuronal culture

- ○ Culture of human iPSCs and differentiation into cortical neurons
- ● METHOD DETAILS
  - ○ In vitro plasmid transfection and adenoviral transduction
  - ○ Control diet and ketogenic diet
  - ○ Cell viability assay
  - ○ Targeted metabolic profiling and metabolic pathway analysis
  - ○ Cell and tissue-based luciferase assays
  - ○ Quantitative real-time PCR
  - ○ Immunoblot analysis
  - ○ RNA sequencing and analysis
  - ○ Chromatin immunoprecipitation sequencing (ChIP-seq)
  - ○ ChIP-seq data analysis
  - ○ Electrophysiology
  - ○ In vivo drug and viral administration
  - ○ Filament MCAO model of ischemic stroke in mouse
  - ○ Stereotaxic intracerebroventricular administration of 2-DG
  - ○ In vivo bioluminescence imaging
  - ○ Assessment of urine ketone body and other physiological parameters
  - ○ Behavioral analysis
- ● QUANTIFICATION AND STATISTICAL ANALYSIS

SUPPLEMENTAL INFORMATION

Supplemental information can be found online at https://doi.org/10.1016/j.neuron.2023.06.013.

AUTHOR CONTRIBUTIONS

Conceptualization, A.K. and R.R.R.; investigation, A.K., S.S.K., C.C., Y.C., R.K., Y.C., and Z.W.; writing – original draft, A.K. and R.R.R.; visualization, A.K.; writing – review & editing, A.K., S.S.K., C.C., R.K., Y.C., M.B., B.T.S., Z.W., C.S., S.C., G.-L.M., J.T., T.T., and R.R.R.; funding acquisition, A.K. and R.R.R.; resources, S.C., J.T., and T.T.; project administration, A.K. and R.R.R.; feedback and expert suggestions, M.B., B.T.S., G.-L.M., J.T., T.T., D.H.G., and R.R.R.

DECLARATION OF INTERESTS

R.R.R. is a stakeholder of Neuronasal and a member of its Scientific Advisory Board. He is also a member of the Scientific Advisory Board for Elevian. The Burke Neurological Institute has filed a provisional patent related to the work presented in this manuscript.

INCLUSION AND DIVERSITY

We support inclusive, diverse, and equitable conduct of research.

REFERENCES

1. Younes, L., Albert, M., Moghekar, A., Soldan, A., Pettigrew, C., and Miller, M.I. (2019). Identifying changepoints in biomarkers during the preclinical phase of Alzheimer's disease. Front. Aging Neurosci. 11, 74. https://doi.org/10.3389/fnagi.2019.00074.

2. Jack, C.R., Jr., Lowe, V.J., Weigand, S.D., Wiste, H.J., Senjem, M.L., Knopman, D.S., Shiung, M.M., Gunter, J.L., Boeve, B.F., Kemp, B.J., et al. (2009). Serial PIB and MRI in normal, mild cognitive impairment and Alzheimer's disease: implications for sequence of pathological events in Alzheimer's disease. Brain 132, 1355–1365. https://doi.org/10.1093/brain/awp062.

3. Duan, W., and Mattson, M.P. (1999). Dietary restriction and 2-deoxyglucose administration improve behavioral outcome and reduce degeneration of dopaminergic neurons in models of Parkinson's disease. J. Neurosci. Res. 57, 195–206. https://doi.org/10.1002/(SICI)1097-4547(19990715)57:2<195::AID-JNR5>3.0.CO;2-P.

4. Johnson, J.B., Summer, W., Cutler, R.G., Martin, B., Hyun, D.H., Dixit, V.D., Pearson, M., Nassar, M., Telljohann, R., Maudsley, S., et al. (2007). Alternate day calorie restriction improves clinical findings and reduces markers of oxidative stress and inflammation in overweight adults with moderate asthma. Free Radic. Biol. Med. 42, 665–674. https://doi.org/10.1016/j.freeradbiomed.2006.12.005.

5. Courchesne-Loyer, A., Croteau, E., Castellano, C.A., St-Pierre, V., Hennebelle, M., and Cunnane, S.C. (2017). Inverse relationship between brain glucose and ketone metabolism in adults during short-term moderate dietary ketosis: A dual tracer quantitative positron emission tomography study. J. Cereb. Blood Flow Metab. 37, 2485–2493. https://doi.org/10.1177/0271678X16669366.

6. Li, L., Wang, Z., and Zuo, Z. (2013). Chronic intermittent fasting improves cognitive functions and brain structures in mice. PLoS One 8, e66069. https://doi.org/10.1371/journal.pone.0066069.

7. Fontán-Lozano, A., Sáez-Cassanelli, J.L., Inda, M.C., de los Santos-Arteaga, M., Sierra-Domínguez, S.A., López-Lluch, G., Delgado-García, J.M., and Carrión, A.M. (2007). Caloric restriction increases learning consolidation and facilitates synaptic plasticity through mechanisms dependent on NR2B subunits of the NMDA receptor. J. Neurosci. 27, 10185–10195. https://doi.org/10.1523/JNEUROSCI.2757-07.2007.

8. Halagappa, V.K., Guo, Z., Pearson, M., Matsuoka, Y., Cutler, R.G., Laferla, F.M., and Mattson, M.P. (2007). Intermittent fasting and caloric restriction ameliorate age-related behavioral deficits in the triple-transgenic mouse model of Alzheimer's disease. Neurobiol. Dis. 26, 212–220. https://doi.org/10.1016/j.nbd.2006.12.019.

9. Zhang, J., Zhan, Z., Li, X., Xing, A., Jiang, C., Chen, Y., Shi, W., and An, L. (2017). Intermittent fasting protects against Alzheimer's disease possible through restoring Aquaporin-4 polarity. Front. Mol. Neurosci. 10, 395. https://doi.org/10.3389/fnmol.2017.00395.

10. Shin, B.K., Kang, S., Kim, D.S., and Park, S. (2018). Intermittent fasting protects against the deterioration of cognitive function, energy metabolism and dyslipidemia in Alzheimer's disease-induced estrogen deficient rats. Exp. Biol. Med. (Maywood) 243, 334–343. https://doi.org/10.1177/1535370217751610.

11. Ooi, T.C., Meramat, A., Rajab, N.F., Shahar, S., Ismail, I.S., Azam, A.A., and Sharif, R. (2020). Intermittent fasting enhanced the cognitive function in older adults with mild cognitive impairment by inducing biochemical and metabolic changes: a 3-year progressive study. Nutrients 12. https://doi.org/10.3390/nu12092644.

12. Currenti, W., Godos, J., Castellano, S., Caruso, G., Ferri, R., Caraci, F., Grosso, G., and Galvano, F. (2021). Association between time restricted

feeding and cognitive status in older Italian adults. Nutrients *13*. https://doi.org/10.3390/nu13010191.

13. Mattson, M.P., Moehl, K., Ghena, N., Schmaedick, M., and Cheng, A. (2018). Intermittent metabolic switching, neuroplasticity and brain health. Nat. Rev. Neurosci. *19*, 63–80. https://doi.org/10.1038/nrn.2017.156.

14. Hasan-Olive, M.M., Lauritzen, K.H., Ali, M., Rasmussen, L.J., Storm-Mathisen, J., and Bergersen, L.H. (2019). A ketogenic diet improves mitochondrial biogenesis and bioenergetics via the PGC1alpha-SIRT3-UCP2 axis. Neurochem. Res. *44*, 22–37. https://doi.org/10.1007/s11064-018-2588-6.

15. Youm, Y.H., Nguyen, K.Y., Grant, R.W., Goldberg, E.L., Bodogai, M., Kim, D., D'Agostino, D., Planavsky, N., Lupfer, C., Kanneganti, T.D., et al. (2015). The ketone metabolite beta-hydroxybutyrate blocks NLRP3 inflammasome-mediated inflammatory disease. Nat. Med. *21*, 263–269. https://doi.org/10.1038/nm.3804.

16. Finn, P.F., and Dice, J.F. (2005). Ketone bodies stimulate chaperone-mediated autophagy. J. Biol. Chem. *280*, 25864–25870. https://doi.org/10.1074/jbc.M502456200.

17. Marosi, K., Kim, S.W., Moehl, K., Scheibye-Knudsen, M., Cheng, A., Cutler, R., Camandola, S., and Mattson, M.P. (2016). 3-hydroxybutyrate regulates energy metabolism and induces BDNF expression in cerebral cortical neurons. J. Neurochem. *139*, 769–781. https://doi.org/10.1111/jnc.13868.

18. Sleiman, S.F., Henry, J., Al-Haddad, R., El Hayek, L., Abou Haidar, E., Stringer, T., Ulja, D., Karuppagounder, S.S., Holson, E.B., Ratan, R.R., et al. (2016). Exercise promotes the expression of brain derived neurotrophic factor (BDNF) through the action of the ketone body beta-hydroxybutyrate. eLife *5*. https://doi.org/10.7554/eLife.15092.

19. Wan, R., Camandola, S., and Mattson, M.P. (2004). Dietary supplementation with 2-deoxy-D-glucose improves cardiovascular and neuroendocrine stress adaptation in rats. Am. J. Physiol. Heart Circ. Physiol. *287*, H1186–H1193. https://doi.org/10.1152/ajpheart.00932.2003.

20. Tower, D.B. (1958). The effects of 2-deoxy-D-glucose on metabolism of slices of cerebral cortex incubated in vitro. J. Neurochem. *3*, 185–205. https://doi.org/10.1111/j.1471-4159.1958.tb12625.x.

21. Bachelard, H.S. (1971). Specificity and kinetic properties of monosaccharide uptake into guinea pig cerebral cortex in vitro. J. Neurochem. *18*, 213–222. https://doi.org/10.1111/j.1471-4159.1971.tb00559.x.

22. Horton, R.W., Meldrum, B.S., and Bachelard, H.S. (1973). Enzymic and cerebral metabolic effects of 2-deoxy-D-glucose. J. Neurochem. *21*, 507–520. https://doi.org/10.1111/j.1471-4159.1973.tb05996.x.

23. Bertoni, J.M. (1981). Competitive inhibition of rat brain hexokinase by 2-deoxyglucose, glucosamine, and metrizamide. J. Neurochem. *37*, 1523–1528. https://doi.org/10.1111/j.1471-4159.1981.tb06322.x.

24. Garriga-Canut, M., Schoenike, B., Qazi, R., Bergendahl, K., Daley, T.J., Pfender, R.M., Morrison, J.F., Ockuly, J., Stafstrom, C., Sutula, T., et al. (2006). 2-deoxy-D-glucose reduces epilepsy progression by NRSF-CtBP-dependent metabolic regulation of chromatin structure. Nat. Neurosci. *9*, 1382–1387. https://doi.org/10.1038/nn1791.

25. Yao, J., Chen, S., Mao, Z., Cadenas, E., and Brinton, R.D. (2011). 2-Deoxy-D-glucose treatment induces ketogenesis, sustains mitochondrial function, and reduces pathology in female mouse model of Alzheimer's disease. PLoS One *6*, e21788. https://doi.org/10.1371/journal.pone.0021788.

26. Suzuki, A., Fukushima, H., Mukawa, T., Toyoda, H., Wu, L.J., Zhao, M.G., Xu, H., Shang, Y., Endoh, K., Iwamoto, T., et al. (2011). Upregulation of CREB-mediated transcription enhances both short- and long-term memory. J. Neurosci. *31*, 8786–8802. https://doi.org/10.1523/JNEUROSCI.3257-10.2011.

27. Pavlopoulos, E., Jones, S., Kosmidis, S., Close, M., Kim, C., Kovalerchik, O., Small, S.A., and Kandel, E.R. (2013). Molecular mechanism for age-related memory loss: the histone-binding protein RbAp48. Sci. Transl. Med. *5*, 200ra115. https://doi.org/10.1126/scitranslmed.3006373.

28. Zafra, F., Hengerer, B., Leibrock, J., Thoenen, H., and Lindholm, D. (1990). Activity dependent regulation of BDNF and NGF mRNAs in the rat hippocampus is mediated by non-NMDA glutamate receptors. EMBO J. *9*, 3545–3550. https://doi.org/10.1002/j.1460-2075.1990.tb07564.x.

29. Ghosh, A., Carnahan, J., and Greenberg, M.E. (1994). Requirement for BDNF in activity-dependent survival of cortical neurons. Science *263*, 1618–1623. https://doi.org/10.1126/science.7907431.

30. Murphy, T.H., and Baraban, J.M. (1990). Glutamate toxicity in immature cortical neurons precedes development ofglutamate receptor currents. Dev. Brain Res. *57*, 146–150.

31. Wen, Z., Nguyen, H.N., Guo, Z., Lalli, M.A., Wang, X., Su, Y., Kim, N.S., Yoon, K.J., Shin, J., Zhang, C., et al. (2014). Synaptic dysregulation in a human iPS cell model of mental disorders. Nature *515*, 414–418. https://doi.org/10.1038/nature13716.

32. Yu, Z.F., and Mattson, M.P. (1999). Dietary restriction and 2-deoxyglucose administration reduce focal ischemic brain damage and improve behavioral outcome: evidence for a preconditioning mechanism. J. Neurosci. Res. *57*, 830–839.

33. Stuart, C.A., Ross, I.R., Howell, M.E., McCurry, M.P., Wood, T.G., Ceci, J.D., Kennel, S.J., and Wall, J. (2011). Brain glucose transporter (Glut3) haploinsufficiency does not impair mouse brain glucose uptake. Brain Res. *1384*, 15–22. https://doi.org/10.1016/j.brainres.2011.02.014.

34. Pang, P.T., Teng, H.K., Zaitsev, E., Woo, N.T., Sakata, K., Zhen, S., Teng, K.K., Yung, W.H., Hempstead, B.L., and Lu, B. (2004). Cleavage of proBDNF by tPA/plasmin is essential for long-term hippocampal plasticity. Science *306*, 487–491. https://doi.org/10.1126/science.1100135.

35. Fluri, F., Schuhmann, M.K., and Kleinschnitz, C. (2015). Animal models of ischemic stroke and their application in clinical research. Drug Des. Devel. Ther. *9*, 3445–3454. https://doi.org/10.2147/DDDT.S56071.

36. Karuppagounder, S.S., Alin, L., Chen, Y., Brand, D., Bourassa, M.W., Dietrich, K., Wilkinson, C.M., Nadeau, C.A., Kumar, A., Perry, S., et al. (2018). N-acetylcysteine targets 5 lipoxygenase-derived, toxic lipids and can synergize with prostaglandin E2 to inhibit ferroptosis and improve outcomes following hemorrhagic stroke in mice. Ann. Neurol. *84*, 854–872. https://doi.org/10.1002/ana.25356.

37. Glajch, K.E., Fleming, S.M., Surmeier, D.J., and Osten, P. (2012). Sensorimotor assessment of the unilateral 6-hydroxydopamine mouse model of Parkinson;s disease. Behav. Brain Res. *230*, 309–316. https://doi.org/10.1016/j.bbr.2011.12.007.

38. Hock, C., Heese, K., Hulette, C., Rosenberg, C., and Otten, U. (2000). Region-specific neurotrophin imbalances in Alzheimer disease: decreased levels of brain-derived neurotrophic factor and increased levels of nerve growth factor in hippocampus and cortical areas. Arch. Neurol. *57*, 846–851. https://doi.org/10.1001/archneur.57.6.846.

39. Nagahara, A.H., Merrill, D.A., Coppola, G., Tsukada, S., Schroeder, B.E., Shaked, G.M., Wang, L., Blesch, A., Kim, A., Conner, J.M., et al. (2009). Neuroprotective effects of brain-derived neurotrophic factor in rodent and primate models of Alzheimer's disease. Nat. Med. *15*, 331–337. https://doi.org/10.1038/nm.1912.

40. Choi, S.H., Bylykbashi, E., Chatila, Z.K., Lee, S.W., Pulli, B., Clemenson, G.D., Kim, E., Rompala, A., Oram, M.K., Asselin, C., et al. (2018). Combined adult neurogenesis and BDNF mimic exercise effects on cognition in an Alzheimer's mouse model. Science *361*. https://doi.org/10.1126/science.aan8821.

41. Hüttenrauch, M., Baches, S., Gerth, J., Bayer, T.A., Weggen, S., and Wirths, O. (2015). Neprilysin deficiency alters the neuropathological and behavioral phenotype in the 5XFAD mouse model of Alzheimer's disease. J. Alzheimers Dis. *44*, 1291–1302. https://doi.org/10.3233/JAD-142463.

42. Devi, L., and Ohno, M. (2010). Phospho-eIF2alpha level is important for determining abilities of BACE1 reduction to rescue cholinergic neurodegeneration and memory defects in 5XFAD mice. PLoS One *5*, e12974. https://doi.org/10.1371/journal.pone.0012974.

43. Xiao, N.A., Zhang, J., Zhou, M., Wei, Z., Wu, X.L., Dai, X.M., Zhu, Y.G., and Chen, X.C. (2015). Reduction of glucose metabolism in olfactory bulb is an earlier Alzheimer's disease-related biomarker in 5XFAD mice. Chin. Med. J. (Engl) 128, 2220–2227. https://doi.org/10.4103/0366-6999.162507.

44. Serralta, A., Barcia, J.A., Ortiz, P., Durán, C., Hernández, M.E., and Alós, M. (2006). Effect of intracerebroventricular continuous infusion of valproic acid versus single i.p. and i.c.v. injections in the amygdala kindling epilepsy model. Epilepsy Res. 70, 15–26. https://doi.org/10.1016/j.eplepsyres.2006.02.003.

45. Hardie, D.G. (2011). AMP-activated protein kinase: an energy sensor that regulates all aspects of cell function. Genes Dev. 25, 1895–1908. https://doi.org/10.1101/gad.17420111.

46. Kumar, A. (2019). Sugar as a therapeutic target for the cognitive restoration following traumatic brain injury. Curr. Opin. Neurol. 32, 815–821. https://doi.org/10.1097/WCO.0000000000000752.

47. Lu, C., and Thompson, C.B. (2012). Metabolic regulation of epigenetics. Cell Metab. 16, 9–17. https://doi.org/10.1016/j.cmet.2012.06.001.

48. Ratan, R.R., Murphy, T.H., and Baraban, J.M. (1994). Macromolecular synthesis inhibitors prevent oxidative stress-induced apoptosis in embryonic cortical neurons by shunting cysteine from protein synthesis to glutathione. J. Neurosci. 14, 4385–4392.

49. Martínez, G., Vidal, R.L., Mardones, P., Serrano, F.G., Ardiles, A.O., Wirth, C., Valdés, P., Thielen, P., Schneider, B.L., Kerr, B., et al. (2016). Regulation of memory formation by the transcription factor XBP1. Cell Rep. 14, 1382–1394. https://doi.org/10.1016/j.celrep.2016.01.028.

50. Pasini, S., Corona, C., Liu, J., Greene, L.A., and Shelanski, M.L. (2015). Specific downregulation of hippocampal ATF4 reveals a necessary role in synaptic plasticity and memory. Cell Rep. 11, 183–191. https://doi.org/10.1016/j.celrep.2015.03.025.

51. Lange, P.S., Chavez, J.C., Pinto, J.T., Coppola, G., Sun, C.W., Townes, T.M., Geschwind, D.H., and Ratan, R.R. (2008). ATF4 is an oxidative stress-inducible, prodeath transcription factor in neurons in vitro and in vivo. J. Exp. Med. 205, 1227–1242. https://doi.org/10.1084/jem.20071460.

52. Karuppagounder, S.S., Alim, I., Khim, S.J., Bourassa, M.W., Sleiman, S.F., John, R., Thinnes, C.C., Yeh, T.L., Demetriades, M., Neitemeier, S., et al. (2016). Therapeutic targeting of oxygen-sensing prolyl hydroxylases abrogates ATF4-dependent neuronal death and improves outcomes after brain hemorrhage in several rodent models. Sci. Transl. Med. 8, 328ra29. https://doi.org/10.1126/scitranslmed.aac6008.

53. Breitling, J., and Aebi, M. (2013). N-linked protein glycosylation in the endoplasmic reticulum. Cold Spring Harb. Perspect. Biol. 5, a013359. https://doi.org/10.1101/cshperspect.a013359.

54. Surani, M.A. (1979). Glycoprotein synthesis and inhibition of glycosylation by tunicamycin in preimplantation mouse embryos: compaction and trophoblast adhesion. Cell 18, 217–227. https://doi.org/10.1016/0092-8674(79)90370-2.

55. Pitera, A.P., Asuni, A.A., O'Connor, V., and Deinhardt, K. (2019). Pathogenic tau does not drive activation of the unfolded protein response. J. Biol. Chem. 294, 9679–9688. https://doi.org/10.1074/jbc.RA119.008263.

56. Axten, J.M., Medina, J.R., Feng, Y., Shu, A., Romeril, S.P., Grant, S.W., Li, W.H., Heerding, D.A., Minthorn, E., Mencken, T., et al. (2012). Discovery of 7-methyl-5-(1-{[3-(trifluoromethyl)phenylacetyl]-2,3-dihydro-1H-indol-5-yl)-7H-p yrrolo[2,3-d]pyrimidin-4-amine (GSK2606414), a potent and selective first-in-class inhibitor of protein kinase R (PKR)-like endoplasmic reticulum kinase (PERK). J Med Chem 55, 7193–7207. https://doi.org/10.1021/jm300713s.

57. So, J.S., Cho, S., Min, S.H., Kimball, S.R., and Lee, A.H. (2015). IRE1alpha-dependent decay of CReP/Ppp1r15b mRNA increases eukaryotic initiation factor 2alpha phosphorylation and suppresses protein synthesis. Mol. Cell. Biol. 35, 2761–2770. https://doi.org/10.1128/MCB.00215-15.

58. Alim, I., Caulfield, J.T., Chen, Y., Swarup, V., Geschwind, D.H., Ivanova, E., Seravalli, J., Ai, Y., Sansing, L.H., Ste Marie, E.J., et al. (2019). Selenium drives a transcriptional adaptive program to block ferroptosis and treat stroke. Cell 177, 1262–1279.e25. https://doi.org/10.1016/j.cell.2019.03.032.

59. Tuvikene, J., Esvald, E.E., Rähni, A., Uustalu, K., Zhuravskaya, A., Avarlaid, A., Makeyev, E.V., and Timmusk, T. (2021). Intronic enhancer region governs transcript-specific Bdnf expression in rodent neurons. eLife 10. https://doi.org/10.7554/eLife.65161.

60. Heinz, S., Benner, C., Spann, N., Bertolino, E., Lin, Y.C., Laslo, P., Cheng, J.X., Murre, C., Singh, H., and Glass, C.K. (2010). Simple combinations of lineage-determining transcription factors prime cis-regulatory elements required for macrophage and B cell identities. Mol. Cell 38, 576–589. https://doi.org/10.1016/j.molcel.2010.05.004.

61. Fujii, Y., Shimizu, T., Toda, T., Yanagida, M., and Hakoshima, T. (2000). Structural basis for the diversity of DNA recognition by bZIP transcription factors. Nat. Struct. Biol. 7, 889–893. https://doi.org/10.1038/82822.

62. Tian, F., Cheng, Y., Zhou, S., Wang, Q., Monavarfeshani, A., Gao, K., Jiang, W., Kawaguchi, R., Wang, Q., Tang, M., et al. (2022). Core transcription programs controlling injury-induced neurodegeneration of retinal ganglion cells. Neuron 110, 2607–2624.e8. https://doi.org/10.1016/j.neuron.2022.06.003.

63. Huggins, C.J., Mayekar, M.K., Martin, N., Saylor, K.L., Gonit, M., Jailwala, P., Kasoji, M., Haines, D.C., Quiñones, O.A., and Johnson, P.F. (2015). C/EBPgamma is a critical regulator of cellular stress response networks through heterodimerization with ATF4. Mol. Cell. Biol. 36, 693–713. https://doi.org/10.1128/MCB.00911-15.

64. Kanikarla-Marie, P., and Jain, S.K. (2016). Hyperketonemia and ketosis increase the risk of complications in type 1 diabetes. Free Radic. Biol. Med. 95, 268–277. https://doi.org/10.1016/j.freeradbiomed.2016.03.020.

65. Datema, R., and Schwarz, R.T. (1978). Formation of 2-deoxyglucose-containing lipid-linked oligosaccharides. Interference with glycosylation of glycoproteins. Eur. J. Biochem. 90, 505–516. https://doi.org/10.1111/j.1432-1033.1978.tb12630.x.

66. Miyahara, H., Hasegawa, K., Yashiro, M., Ohara, T., Fujisawa, M., Yoshimura, T., Matsukawa, A., and Tsukahara, H. (2022). Thioredoxin interacting protein protects mice from fasting induced liver steatosis by activating ER stress and its downstream signaling pathways. Sci. Rep. 12, 4819. https://doi.org/10.1038/s41598-022-08791-z.

67. Sokolović, M., Sokolović, A., Wehkamp, D., Ver Loren van Themaat, E., de Waart, D.R., Gilhuijs-Pederson, L.A., Nikolsky, Y., van Kampen, A.H., Hakvoort, T.B., and Lamers, W.H. (2008). The transcriptomic signature of fasting murine liver. BMC Genomics 9, 528. https://doi.org/10.1186/1471-2164-9-528.

68. Vattem, K.M., and Wek, R.C. (2004). Reinitiation involving upstream ORFs regulates ATF4 mRNA translation in mammalian cells. Proc. Natl. Acad. Sci. USA 101, 11269–11274. https://doi.org/10.1073/pnas.0400541101.

69. Bartsch, D., Ghirardi, M., Skehel, P.A., Karl, K.A., Herder, S.P., Chen, M., Bailey, C.H., and Kandel, E.R. (1995). Aplysia CREB2 represses long-term facilitation: relief of repression converts transient facilitation into long-term functional and structural change. Cell 83, 979–992. https://doi.org/10.1016/0092-8674(95)90213-9.

70. Chen, A., Muzzio, I.A., Malleret, G., Bartsch, D., Verbitsky, M., Pavlidis, P., Yonan, A.L., Vronskaya, S., Grody, M.B., Cepeda, I., et al. (2003). Inducible enhancement of memory storage and synaptic plasticity in transgenic mice expressing an inhibitor of ATF4 (CREB-2) and C/EBP proteins. Neuron 39, 655–669. https://doi.org/10.1016/S0896-6273(03)00501-4.

71. Costa-Mattioli, M., Gobert, D., Harding, H., Herdy, B., Azzi, M., Bruno, M., Bidinosti, M., Ben Mamou, C., Marcinkiewicz, E., Yoshida, M., et al. (2005). Translational control of hippocampal synaptic plasticity and memory by the eIF2alpha kinase GCN2. Nature 436, 1166–1173. https://doi.org/10.1038/nature03897.

72. Costa-Mattioli, M., Gobert, D., Stern, E., Gamache, K., Colina, R., Cuello, C., Sossin, W., Kaufman, R., Pelletier, J., Rosenblum, K., et al. (2007). eIF2alpha phosphorylation bidirectionally regulates the switch from

short- to long-term synaptic plasticity and memory. Cell *129*, 195–206. https://doi.org/10.1016/j.cell.2007.01.050.

73. Jiang, Z., Belforte, J.E., Lu, Y., Yabe, Y., Pickel, J., Smith, C.B., Je, H.S., Lu, B., and Nakazawa, K. (2010). eIF2alpha Phosphorylation-dependent translation in CA1 pyramidal cells impairs hippocampal memory consolidation without affecting general translation. J. Neurosci. *30*, 2582–2594. https://doi.org/10.1523/JNEUROSCI.3971-09.2010.

74. Ma, T., Trinh, M.A., Wexler, A.J., Bourbon, C., Gatti, E., Pierre, P., Cavener, D.R., and Klann, E. (2013). Suppression of eIF2alpha kinases alleviates Alzheimer's disease-related plasticity and memory deficits. Nat. Neurosci. *16*, 1299–1305. https://doi.org/10.1038/nn.3486.

75. Raez, L.E., Papadopoulos, K., Ricart, A.D., Chiorean, E.G., Dipaola, R.S., Stein, M.N., Rocha Lima, C.M., Schlesselman, J.J., Tolba, K., Langmuir, V.K., et al. (2013). A phase I dose-escalation trial of 2-deoxy-D-glucose alone or combined with docetaxel in patients with advanced solid tumors. Cancer Chemother. Pharmacol. *71*, 523–530. https://doi.org/10.1007/s00280-012-2045-1.

76. Stein, M., Lin, H., Jeyamohan, C., Dvorzhinski, D., Gounder, M., Bray, K., Eddy, S., Goodin, S., White, E., and Dipaola, R.S. (2010). Targeting tumor metabolism with 2-deoxyglucose in patients with castrate-resistant prostate cancer and advanced malignancies. Prostate *70*, 1388–1394. https://doi.org/10.1002/pros.21172.

77. Nair, A.B., and Jacob, S. (2016). A simple practice guide for dose conversion between animals and human. J. Basic Clin. Pharm. *7*, 27–31. https://doi.org/10.4103/0976-0105.177703.

78. Dobin, A., Davis, C.A., Schlesinger, F., Drenkow, J., Zaleski, C., Jha, S., Batut, P., Chaisson, M., and Gingeras, T.R. (2013). STAR: ultrafast universal RNA-seq aligner. Bioinformatics *29*, 15–21. https://doi.org/10.1093/bioinformatics/bts635.

79. Anders, S., Pyl, P.T., and Huber, W. (2015). HTSeq–a Python framework to work with high-throughput sequencing data. Bioinformatics *31*, 166–169. https://doi.org/10.1093/bioinformatics/btu638.

80. Robinson, M.D., McCarthy, D.J., and Smyth, G.K. (2010). edgeR: a Bioconductor package for differential expression analysis of digital gene expression data. Bioinformatics *26*, 139–140. https://doi.org/10.1093/bioinformatics/btp616.

81. Li, H., and Durbin, R. (2009). Fast and accurate short read alignment with Burrows-Wheeler transform. Bioinformatics *25*, 1754–1760. https://doi.org/10.1093/bioinformatics/btp324.

82. Ramírez, F., Ryan, D.P., Grüning, B., Bhardwaj, V., Kilpert, F., Richter, A.S., Heyne, S., Dündar, F., and Manke, T. (2016). deepTools2: a next generation web server for deep-sequencing data analysis. Nucleic Acids Res. *44*, W160–W165. https://doi.org/10.1093/nar/gkw257.

83. Zhang, Y., Liu, T., Meyer, C.A., Eeckhoute, J., Johnson, D.S., Bernstein, B.E., Nusbaum, C., Myers, R.M., Brown, M., Li, W., et al. (2008). Model-based analysis of ChIP-Seq (MACS). Genome Biol. *9*, R137. https://doi.org/10.1186/gb-2008-9-9-r137.

84. Stark, R., and Brown, G. (2011). DiffBind: differential binding analysis of ChIPSeq peak data. (Bioconductor). https://bioconductor.org/packages/devel/bioc/vignettes/DiffBind/inst/doc/DiffBind.pdf.

85. Sandelin, A., Alkema, W., Engström, P., Wasserman, W.W., and Lenhard, B. (2004). JASPAR: an open-access database for eukaryotic transcription factor binding profiles. Nucleic Acids Res. *32*, D91–D94. https://doi.org/10.1093/nar/gkh012.

86. Ratan, R.R., Murphy, T.H., and Baraban, J.M. (1994). Oxidative stress induces apoptosis in embryonic cortical neurons. J. Neurochem. *62*, 376–379. https://doi.org/10.1046/j.1471-4159.1994.62010376.x.

87. Chen, W.W., Freinkman, E., Wang, T., Birsoy, K., and Sabatini, D.M. (2016). Absolute quantification of matrix metabolites reveals the dynamics of mitochondrial metabolism. Cell *166*, 1324–1337.e11. https://doi.org/10.1016/j.cell.2016.07.040.

88. Balkaya, M., Kröber, J.M., Rex, A., and Endres, M. (2013). Assessing post-stroke behavior in mouse models of focal ischemia. J. Cereb. Blood Flow Metab. *33*, 330–338. https://doi.org/10.1038/jcbfm.2012.185.

STAR★METHODS

KEY RESOURCES TABLE

REAGENT or RESOURCE	SOURCE	IDENTIFIER
Antibodies		
Anti-Glut3	Abcam	Cat# ab41525; RRID: AB_732609
Anti-β-actin	Sigma-Aldrich	Cat# A5316; RRID: AB_476743
Anti-BDNF (N-20)	Santa Cruz Biotechnology	Cat# sc-546; RRID: AB_630940
Anti-α-tubulin	Sigma-Aldrich	Cat# T8203; RRID: AB_1841230
Anti-phospho-AMPKα (Thr 172)	Cell Signaling Technology	Cat# 2535; RRID: AB_331250
Anti-AMPKα	Cell Signaling Technology	Cat# 2532; RRID: AB_330331
Anti-GFP	Cell Signaling Technology	Cat# 2555; RRID: AB_10692764
Anti-phospho-EIF2S1 (S51)	Abcam	Cat# ab32157; RRID: AB_732117
Anti-eIF2α	Cell Signaling Technology	Cat# 9722S; RRID: AB_2230924
Anti-ATF4	Millipore	Cat# ABE387
Bacterial and virus strains		
Ad-CMV GFP	ViraQuest, Inc. (North liberty, IA)	MSRN: 22576
Ad-AMPKα1 D.N.	ViraQuest, Inc. (North liberty, IA)	MSRN: 17930
AAV8-EGFP-iCre	Vector Biolabs	7097
AAV8-GFP	Vector Biolabs	7061
AAV9-CamKII(0.4)-EGFP-T2A-iCre-WPRE	Vector Biolabs	VB5191
AAV9-CamkII(0.4)-eGFP-WPRE	Vector Biolabs	VB5206
Ad-mATF4 d-RK	ViraQuest, Inc. (North liberty, IA)	25195
Ad-mATF4 WT	ViraQuest, Inc. (North liberty, IA)	22902
Biological samples		
Primary cortical neurons from CD-1 strain mice	Charles River	See "Experimental model details" section
Human iPSC line (C1-1) was previously generated from skin biopsy samples of male newborn and had been fully characterized and passaged on MEF feeder layers	See Wen et al.[31]	See "Experimental model details" section
CD1 mice	Charles River	See "Experimental model details" section
C57BL/6 mice	Charles River	See "Experimental model details" section
5xFAD mice	Jackson's laboratory	Stock Number# 034848-JAX
Ppp1R15b$^{fl/fl}$ mice	Generous gifted from Ann-Hwee Lee (Regeneron Pharmaceuticals)	See "Experimental model details" section
C57BL/6-ATF4$^{tm1.1Cmad}$/J	Jackson's laboratory	Strain Number# 033380
Chemicals, peptides, and recombinant proteins		
2-Deoxyglucose	Sigma-Aldrich	Cat# D6134; CAS Number 154-17-6
Lonidamine	Tocris	Cat# 1646; CAS number 50264-69-2
Collagenase Type VII-S	Sigma-Aldrich	Cat# C2399; CAS Number 9001-12-1
Diluent Sodium chloride (0.9% solution)	Hospira	Cat# 00409488820
Metformin	Sigma-Aldrich	Cat# D150959; CAS Number 1115-70-4
Actinomycin D	Sigma-Aldrich	Cat# AA1410; CAS Number 50-76-0
Tunicamycin	Sigma-Aldrich	Cat# T7765; CAS Number 11089-65-9
GSK2606414 (PERK inhibitor I)	Sigma-Aldrich	Cat# 516535; CAS Number 1337531-89-1
2-Mercaptoethanol	Sigma-Aldrich	Cat# M3148; CAS Number 60-24-2
1,4-Dithiothreitol (DTT)	ThermoFisher Scientific	Cat# R0861; CAS Number 3483-12-3

Continued

REAGENT or RESOURCE	SOURCE	IDENTIFIER
Triton X-100	Sigma-Aldrich	Cat# X100; CAS Number 9002-93-1
Protease Inhibitor Cocktail	Sigma-Aldrich	Cat# P8340
Pheylmethanesulfonyl fluoride (PMSF)	Sigma-Aldrich	Cat# P8340; CAS Number 329-98-6
Ethylene glycol-bis(2aminoehylether)-N, N, N, N-tetra acetic acid (EGTA)	Sigma-Aldrich	Cat# E3889; CAS Number 67-42-5
Trizma base	Sigma-Aldrich	Cat# T4661; CAS Number 77-86-1
Sodium Chloride	Sigma-Aldrich	Cat# S3014; CAS Number 7647-14-5
Potassium chloride	Sigma-Aldrich	Cat# P5405; CAS Number 7447-40-7
Sodium phosphate dibasic	Sigma-Aldrich	Cat# S5136; CAS Number 7558-79-4
Sodium bicarbonate	Sigma-Aldrich	Cat# S6014; CAS Number 144-55-8
D-Glucose	Sigma-Aldrich	Cat# G8270; CAS Number 50-99-7
D-Mannose	Sigma-Aldrich	Cat# M6020; CAS Number 3458-28-4
cOmplete Mini EDTA-free (Protease inhibitor cocktail)	Roche	Cat# 11836170001
16% Formaldehyde, Methanol Free	Cell Signaling Technology	Cat# 12606S
Glycine	Sigma-Aldrich	Cat# 50046; CAS Number: 56-40-6
MG132	Sigma-Aldrich	Cat# M7449; CAS Number: 133407-82-6
UltraPure 1M Tris-HCl, pH 8.0	Invitrogen	Cat# 15568-025
UltraPure 0.5M EDTA, pH 8.0	Invitrogen	Cat# 15575-038
UltraPure 10% SDS	Invitrogen	Cat# 15553-035
Dynabeads Protein G	Invitrogen	Cat# 10003D
5M Sodium chloride solution	Sigma-Aldrich	Cat# 59222C
Sodium-Deoxycholate	ThermoFisher Scientific	Cat# 89904
Lithium chloride solution 8M	Sigma-Aldrich	Cat# L7026
NP-40	ThermoFisher Scientific	Cat# 85124
Critical commercial assays		
Nucleospin RNA Kit	TaKaRa	Cat# 740955.250
MagMAX mirVana Total RNA Isolation Kit	ThermoFisher Scientific	A27828
DC Protein Assay Kit 1	Bio-Rad	5000111
Live/dead Assay kit	ThermoFisher Scientific	L3224
Dual-Luciferase Reporter 1000 Assay System	Promega	E1980
Taqman RNA-to Ct 1-Step kit	ThermoFisher Scientific	4392938
Tagment DNA Enzyme and Buffer	Illumina	20034210
SuperScript III First Strand Synthesis System for RT PCR	Invitrogen	18080-051
SuperScript IV First Strand Synthesis System with ezDNase enzyme	ThermoFisher Scientific	18091050
SYBR Green Master Mix	Applied Biosystems	Cat# 4309155
AMPureXP	Beckman Coulter	Cat# A63880
Fast Ion Plasmid Maxi kit	IBI Scientific	Cat# IB47125
ALZET Brain infusion kit 2 (3-5 mm)	Durect Corporation	Cat# 0008663
ALZET Micro-osmotic pump Model 1004	Durect Corporation	Cat# 0009922
C&B-Metabond Adhesive Cement System	Parkell Inc.	Cat# S380
Ketone test strips	Smackfat Inc.	Cat# 8525184
Deposited Data		
Raw and processed data of RNA Sequencing and ChIP Sequencing	This paper	https://www.ncbi.nlm.nih.gov/geo/query/acc.cgi?acc=GSE217284

(Continued on next page)

Continued

REAGENT or RESOURCE	SOURCE	IDENTIFIER
Oligonucleotides		
FAM labeled *Bdnf* (Taqman probe)	ThermoFisher Scientific	Mm004230607_s1
FAM labeled *Chac1* (Taqman probe)	ThermoFisher Scientific	Mm00509926_m1
FAM labeled *Trib3* (Taqman probe)	ThermoFisher Scientific	Mm00454879_m1
FAM labelled *Ddit3* (Taqman probe)	ThermoFisher Scientific	Mm01135937_g1
FAM labelled *Bip* (Taqman probe)	ThermoFisher Scientific	Mm00517691_m1
Mouse ACTB Control Mix	ThermoFisher Scientific	4351315
BDNF IV-F (GTGAGGTTTGTGTGGACCCC)	ThermoFisher Scientific	N/A
BDNF IV-R (ATTGGGCCGAACTTTCTGGT)	ThermoFisher Scientific	N/A
Gapdh-F (TGGTCTCCTCTGACTTCA ACAGCG)	ThermoFisher Scientific	N/A
Gapdh-R (AGGGGTCTACATGGCAA CTGTGAG)	ThermoFisher Scientific	N/A
+3 kb Bdnf III eRNA-R (CGAAAGCA TCCCAACTCTGC)	ThermoFisher Scientific	N/A
+3 kb eRNA-F (AAACAGGCAGTTGGATCAGA)	ThermoFisher Scientific	N/A
+3 kb eRNA-R (GTAAACCCTGCCCTACGCTC)	ThermoFisher Scientific	N/A
Firefly luciferase-F (GCCATGAAGCGCTA CGCCCTGG)	ThermoFisher Scientific	N/A
Firefly luciferase-R (TCTTGCTCACGAATAC GACGGTGG)	ThermoFisher Scientific	N/A
Renilla luciferase-F (TCAGTGGTGGGCTC GCTGCA)	ThermoFisher Scientific	N/A
Renilla luciferase-R (CTTTGGAAGGTTCA GCAGCTCG)	ThermoFisher Scientific	N/A
5xFAD-FP (5'TCATGACTATCCTCCTGGTGG3')	N/A	N/A
5xFAD-RP (5'CGTTATAGGTTTTAAACA CTTCCCC3')	N/A	N/A
Ppp1r15b-FP (5'CATGCCCAGCTGGAA GTGTTTT3')	N/A	N/A
Ppp1r15b-RP (5'CTGGCCTGAAGCCTG TATGTAAAC3')	N/A	N/A
Recombinant DNA		
Trib3 promoter reporter	Generated in the lab	See Lange et al.,[51] JEM
Mutant Trib3 promoter reporter lacking 33-bp ATF4 binding site	Generated in the lab	See Lange et al.,[51] JEM
pRL-TK-renilla luciferase reporter plasmid	Promega	Cat#E2241
Rat *Bdnf* promoter I with firefly luciferase (No enhancer)	Generated in Timmusk Lab	See Tuvikene et al.,[59] eLIFE
Rat *Bdnf* promoter I with firefly luciferase and +3 kb enhancer region sequence (Forward orientation)	Generated in Timmusk Lab	See Tuvikene et al.,[59] eLIFE
Rat *Bdnf* promoter I with firefly luciferase and +3 kb enhancer region sequence (Reverse orientation)	Generated in Timmusk Lab	See Tuvikene et al.,[59] eLIFE
Rat *Bdnf* promoter I with firefly luciferase and +3 kb enhancer region sequence with ATF4 mutation (Forward orientation)	Generated in Timmusk Lab	See Tuvikene et al.,[59] eLIFE
Rat *Bdnf* promoter I with firefly luciferase and +3 kb enhancer region sequence with ATF4 mutation (Reverse orientation)	Generated in Timmusk Lab	See Tuvikene et al.,[59] eLIFE
pGL4.83 Humanized Renilla luciferase	Promega	N/A

(Continued on next page)

Continued

REAGENT or RESOURCE	SOURCE	IDENTIFIER
Software and algorithms		
ANY-maze 5.1	N/A	N/A
Signal (Version 4.11)	N/A	N/A
Graphpad Prism 9	N/A	N/A
Nikon Digital Sight DS-L3	N/A	N/A
Adobe Illustrator CS6	N/A	N/A
Adobe Photoshop CS6	N/A	N/A
STAR (ver 2.4.0) spliced read aligner	N/A	See Dobin et al.,[78] Bioinformatics
HTSeq.0.6.1	N/A	See Anders et al.,[79] Bioinformatics
EdgeR bioconductor R	N/A	See Robinson et al.,[80] Bioinformatics
Trim Galore	N/A	See https://github.com/FelixKrueger/TrimGalore
BWA-MEM alignment algorithm	N/A	See Li and Durbin,[81] Bioinformatics
Picard MarkDuplicates	N/A	See https://github.com/broadinstitute/picard
deepTools	N/A	See Ramírez et al.,[82] Nucleic Acids Research
MACS2	N/A	See Zhang et al.,[83] Genome Biol
DiffBind	N/A	See Stark and Brown,[84] Bioconductor
HOMER/findMotifsGenome.pl	N/A	See Heinz et al.,[60] Molecular Cell
HOMER and JASPAR database	N/A	See Sandelin et al.,[85] Nucleic Acids Research
UCSC Genome browser	N/A	N/A
XCalibur 4.1	ThermoFisher Scientific	N/A
Other		
Fetal bovine serum	Life Technologies	Cat# 16140-071
Horse serum	Life Technologies	Cat# 26050-088
Penicillin-Streptomycin	Life Technologies	Cat# 15140122
Control diet	Research Diet Inc.	Cat# D07091702
Ketogenic diet	Research Diet Inc.	Cat# D07091701

RESOURCE AVAILABILITY

Lead contact
Further information and requests for resources and reagents should be directed to and will be fulfilled by the lead contact, Rajiv Ratan (rrr2001@med.cornell.edu).

Materials availability
The study did not generate new unique reagents or mouse lines.

Data and code availability
Data reported in this paper are available from the lead contact upon reasonable request. The RNA-sequencing dataset is deposited to Gene Expression Omnibus (GEO: GSE217284). Raw and processed ChIP-seq data are deposited to Gene Expression Omnibus (GEO: GSE217284). This paper does not report original codes. Any additional information required to reanalyze the data reported in this paper is available from the lead contact upon reasonable request.

EXPERIMENTAL MODEL DETAILS

All animal procedures were approved by the Weill Cornell Medicine Institutional Animal Care and Use Committee (Animal protocol: 2014-0029) and conducted in accordance with the NIH Guide for the Care and Use of Laboratory Animals and ARRIVE guidelines. We used C57/BL6 mice for the induction of ischemic stroke. 8-10 weeks old female pregnant CD1 mice were used for primary neuronal culture. Ppp1R15b^fl/fl mice were obtained from Dr. Ann Hwee Lee (Regeneron). The genotypes of Ppp1R15b^fl/fl mice were assessed with PCR using DNA isolated from clipped tails of mice. Twelve-week-old male Ppp1R15b^fl/fl mice were used for inactivation of R15b regulatory subunit of protein phosphatase 1 in the hippocampus through AAV8 GFP or Cre intracranial injection followed by three

weeks of overexpression. Twelve-week-old male and female ATF4^{fl/fl} mice were used for inactivation of hippocampal ATF4 in each hippocampus through the double intracranial injection of AAV9-CamKII GFP or Cre followed by three weeks of overexpression. These mice were purchased from Jackson laboratory (Strain # 033380) and were maintained by breeding male heterozygous transgenic mice with female heterozygous transgenic mice. 5xFAD mice (B6/SJL genetic background) were purchased from Jackson laboratory and was maintained by breeding male heterozygous transgenic mice with wild-type female mice. The 5xFAD mice express human APP and PSEN1 transgenes with a total of five AD-linked mutations: the Swedish (K670N/M671L), Florida (I716V), and London (V717I) mutations in APP, and the M146L and L286V mutations in PSEN1. In the current study, 6-month-old male and female 5XFAD mice and age and sex matched wild-type control (B6/SJL genetic background) were used for memory studies, LTP assessment, and gene expression analyses.

Breeding and genotyping

To maintain the 5xFAD mice colony, male 5xFAD mice were crossed with B6SJLF1/J female mice between 10– 30 weeks of age. To maintain Ppp1r15b mice colony, male homozygous Ppp1r15b mice were crossed with female homozygous Ppp1r15b mice between 10 to 30 weeks of age. For genotyping, 21-day old mice pups were briefly anesthetized by placing them in a mouse anesthetic chamber that is connected to a vaporizer and anesthesia was induced with 3-5% isoflurane mixed with 30% oxygen and 70% nitrogen and a small piece of the tail was cut off with a sharp blade. The tail was cauterized to prevent bleeding. For genotype identification of 5xFAD mouse, PCR was done using primers such as transgene forward primer: 5'TCATGACTATCCTCCTGGTGG3' and transgene reverse primer: 5'CGTTATAGGTTTTAAACACTTCCCC3' and for genotype identification of Ppp1r15b mouse, PCR was done using forward primer: 5'CATGCCCAGCTGGAAGTGTTTT3' and reverse primer: 5'CTGGCCTGAAGCCTGTATGTAAAC3'.

Mouse primary immature cortical neuronal culture

Primary immature neuronal cultures were prepared from cerebral cortex of E14 embryos of CD1 mice under sterile conditions and were cultured as previously described.[48,86]

Culture of human iPSCs and differentiation into cortical neurons

Human iPSC line (C1-1) was previously generated from skin biopsy samples of male newborns and had been fully characterized and passaged on MEF feeder layers.[31] All studies followed institutional IRB and ISCRO protocols approved by University of Pennsylvania Perelman School of Medicine. Human iPSCs were differentiated into cortical neurons following the previously established protocol.[31] Briefly, hiPSCs colonies were detached from the feeder layer with 1 mg/ml collagenase (Thermo Fisher Scientific) treatment for 30 min and suspended in embryonic body (EB) medium, consisting of βFGF-free iPSC medium supplemented with 2 μM Dorsomorphin (Tocris) and 2 μM A-83 (Tocris), in non-treated polystyrene plates for 4 days with a daily medium change. After 4 days, EB medium was replaced by neural induction medium (NPC medium) consisting of DMEM/F12 (Thermo Fisher Scientific), 1X N2 supplement (Thermo Fisher Scientific), 1X MEM NEAA (Thermo Fisher Scientific), 2 μg/ml heparin (Sigma) and 2 μM cyclopamine (Tocris). The floating EBs were then transferred to Matrigel (Corning)-coated 6-well plates at day 7 to form neural tube-like rosettes. The attached rosettes were kept for 15 days with NPC medium change every other day. On day 22, the rosettes were picked mechanically and transferred to low attachment plates (Corning) to form neurospheres in NPC medium containing 1X B27 (Thermo Fisher Scientific). The neurospheres were then dissociated with Accutase (Thermo Fisher Scientific) and placed onto Poly-D-Lysine/laminin (Sigma)-coated coverslips in the neuronal culture medium, consisting of Neurobasal medium (Thermo Fisher Scientific) supplemented with 1X Glutamax (Thermo Fisher Scientific), 1X B27 (Thermo Fisher Scientific), 1 μM cAMP (Sigma), 200 ng/ml L-Ascorbic Acid (Sigma), 10 ng/ml BDNF (PeproTech) and 10 ng/ml GDNF (PeproTech). Half of the medium was replaced once a week during continuous culturing.

METHOD DETAILS

In vitro plasmid transfection and adenoviral transduction

Mouse primary neurons were transduced with adenoviral constructs of GFP (Ad-CMVGFP), AMPK D.N. (Ad-AMPKα1 D.N.), ATF4 (Ad-mATF4 WT) or ATF4ΔRK (Ad-mATF4 Δ-RK) at 200MOI for 4 h in HBSS (Thermo Fisher Scientific, Catalog number – 14025134). Thereafter, HBSS was replaced with MEM, Glutamax supplement containing 10% heat inactivated fetal bovine serum, 5% heat inactivated horse serum, and 1% penicillin/streptomycin. Primary neurons transduced with adenoviral constructs of either an AMPK dominant negative or ATF4 Δ-RK and their respective controls were incubated in this media for 72 h and then treated with 2-DG for a specified time before being harvested for the experiments. Primary neurons transduced with an adenoviral construct of ATF4 and its respective control, GFP were incubated for 24 h and then cells were harvested for the gene expression study.

Control diet and ketogenic diet

8–10-week-old C57/BL6 mice were fed with the control diet (Research Diet Inc., Catalog number: D07091702) or ketogenic diet (Research Diet Inc., Catalog number: D07091701) for three weeks with full access to water.

Cell viability assay

Cell viability of mouse primary neurons treated with increasing concentrations of 2-DG (1mM -15mM) for 6 h was assessed by calcein-acetoxymethyl ester (AM) / ethidium homodimer-1 staining using live/dead viability/cytotoxicity kit (Thermo Fisher Scientific, Catalog number – L3224) using epifluorescence microscopy with inverted microscope Nikon ECLIPSE TS100 attached with digital capture system Nikon digital sight DS-L3.

Targeted metabolic profiling and metabolic pathway analysis

Targeted Metabolite profiling was performed according to a method described in a previous publication.[87] Polar metabolites were extracted using cold 80% methanol. The extracts were dried completely with a Speedvac and redissolved in water before it was applied to the hydrophilic interaction chromatography LC-MS. The sample injection order was randomized. Metabolites were measured on a Q Exactive Orbitrap mass spectrometer (Thermo Scientific), which was coupled to a Vanquish UPLC system (Thermo Scientific) via an Ion Max ion source with a HESI II probe (Thermo Scientific). A Sequant ZIC-pHILIC column (2.1 mm i.d. × 150 mm, particle size of 5 μm, Millipore Sigma) was used for separation of metabolites. A 2.1 × 20 mm guard column with the same packing material was used for protection of the analytical column. Flow rate was set at 150 μL/min. Buffers consisted of 100% acetonitrile for mobile phase A, and 0.1% NH_4OH/20 mM CH_3COONH_4 in water for mobile phase B. The chromatographic gradient ran from 85% to 30% A in 20 min followed by a wash with 30% A and re-equilibration at 85% A. The column temperature was set to 30 °C and the autosampler temperature was set to 4 °C. The Q Exactive was operated in full scan, polarity-switching mode with the following parameters: the spray voltage 3.0 kV, the heated capillary temperature 300 °C, the HESI probe temperature 350 °C, the sheath gas flow 40 units, the auxiliary gas flow 15 units. MS data acquisition was performed in the m/z range of 70–1,000, with 70,000 resolution (at 200 m/z). The AGC target was 3,000,000 and the maximum injection time was 100 ms. The MS data was processed using XCalibur 4.1 (Thermo Scientific) to extract the metabolite signal intensity for relative quantitation. Metabolites were identified using an in-house library established using chemical standards. Identification required exact mass (within 5 ppm) and standard retention times. The final data for AMP/ATP ratio and β-hydroxybutyrate were presented as fold changes relative to control.

Cell and tissue-based luciferase assays

Primary neurons were co-transfected with various plasmids including the Wild-type (WT)*Trib3* promoter or mutant Trib3 promoter lacking the 33 b.p. ATF4 binding site tagged with firefly luciferase and pTK-renilla luciferase plasmid at 1:10 ratio using Lipofectamine 2000 (Thermo Fisher Scientific, catalog number - 11668019) according to the manufacturer's instructions to control for transfection efficiency. Transfected cells were incubated for 24 h and then treated with 2-DG for 6 h. Thereafter, luciferase activity was measured using dual luciferase assay kit (Promega) and bioluminometer (MDS Analytical Technologies). Final luciferase activity was calculated by normalizing firefly luciferase activity with Renilla luciferase activity and then the values were converted to fold change with respect to control. The reporter activities of *Bdnf* promoter I luciferase constructs with or without +3 kb enhancer were measured through mRNA measurement of Firefly luciferase and Renilla Luciferase using two-step RT PCR. The primers used for Firefly luciferase were 5′-GCCATGAAGCGCTACGCCCTGG-3′ and 5′-TCTTGCTCACGAATACGACGGTGG-3′ and for Renilla Luciferase were 5′-TCAGTGGTGGGCTCGCTGCA-3′ and 5′-CTTTGGAAGGTTCAGCAGCTCG-3′. The luciferase activity assay of the brain cortex lysates collected from C57/BL6 mice that expressed CMV 5'UTR ATF4 luciferase reporter was done using the luciferase activity assay kit (Promega). The data was normalized with the total protein estimated with Lowry method using BioRad DC kit (Catalog number: 5000111).

Quantitative real-time PCR

Total RNA was extracted from primary cortical neurons using NucleoSpin RNA II Kit (Clontech, Catalog number – 740955-250). Thereafter, using the Taqman RNA-to-Ct, one step kit (Thermo Fisher Scientific, catalog number - 4392938) and following the manufacturer's instructions, 50 nM of RNA from each sample was mixed with the Taqman® Gene Expression Master Mix and Taqman® Gene Expression Assays for *Bdnf* (Catalog number - Mm04230607_s1), *Bip* (Catalog number - Mm00517691_m1), *Trib3* (Catalog number - Mm00454879_m1), *Chac1* (Catalog number - Mm00509926_m1), and *Ddit3* (Catalog number - Mm01135937_g1) with FAM labelled probe and *Actin* with VIC labelled probe (Catalog number - 4351315) all from Thermo Fisher Scientific on an Applied Biosystems 7500 Fast Real Time PCR System. The gene expression of *Bdnf* exon IV in human i.p.s. derived neurons was assessed using two step qPCR. Total RNA from human i.p.s derived neurons was isolated using mirVana kit (Thermo Fisher Scientific) according to manufacturer's instructions. A total of 1 μg RNA was used to synthesize cDNA with the SuperScript® III First-Strand Synthesis System (Thermo Fisher Scientific). Quantitative real-time PCR was then performed using SYBR green (Applied Biosystems) and the StepOnePlus™ Real-Time PCR System (Applied Biosystems). Quantitative levels for all genes were normalized to the housekeeping gene GAPDH and expressed relative to the relevant control samples. The sequences of primers used in this part of the study were as follows: *BDNF IV* forward: GTGAGGTTTGTGTGGACCCC and *BDNF IV* reverse: ATTGGGCCGAACTTTCTGGT, and *Gapdh* forward: TGGTCTCCTCTGACTTCAACAGCG and *Gapdh* reverse: AGGGGTCTACATGGCAACTGTGAG. cDNA for enhancer RNA (eRNA) was synthesized using SuperScipt IV First Strand Synthesis System with ezDNase enzyme and reverse primers for *Bdnf III* +3 kb eRNA (CGAAAGCATCCCAACTCTGC) and *Gapdh* (AGGGGTCTACATGGCAACTGTGAG). The quantitative real-time PCR was then performed using SYBR green (Thermo Fisher Scientific, Catalog number – 4309155) on an Applied Biosystems 7500 Fast Real Time PCR System. The Quantitative level for eRNA was normalized to the housekeeping gene *Gapdh* and expressed

relative to the relevant control sample as a fold change. The primers used for +3 kb eRNA expression were Fwd: AAACAGGCAGTTGGATCAGA and Rev. GTAAACCCTGCCCTACGCTC and for the *Gapdh* expression, the same primers were used as mentioned above.

Immunoblot analysis
Whole cell proteins were extracted in Triton X-100 lysis buffer (1% Triton X-100, 1% SDS, 50 mM Tris-Cl, pH 7.4, 500 mM NaCl and 1 mM EDTA). Samples were boiled in Laemmli buffer and electrophoresed under reducing conditions on NuPAGE® Novex 4–12% Bis-Tris Gel polyacrylamide gels (Invitrogen). Proteins were transferred to a nitrocellulose membrane (Bio-Rad) by electroblotting. Nonspecific binding was inhibited by incubation in Odyssey blocking buffer (LI-COR Biosciences). Antibodies against Glut3 (Abcam, Catalog no. AB41525, dilution 1:1000), actin (Sigma Aldrich, Catalog no. A5316, dilution 1:10000), BDNF (Santacruz Biotechnology, Catalog no. sc-546, dilution 1:10,000), tubulin (Sigma Aldrich, Catalog no. T8203, dilution 1:10000), p-AMPK (Cell Signaling Technology, Cat no. 2535L, dilution 1:1000), AMPK (Cell Signaling Technology, Cat no. 2532L, dilution 1:1000), GFP (Cell Signaling Technology, Cat no. 2555S, dilution 1:2000), eIF2S1 (phospho S51) (Abcam, Catalog no. AB32157, dilution 1:500), and eIF2α (Cell Signaling Technology, Cat no. 9722, dilution 1:500) were diluted in odyssey blocking buffer and the membranes were incubated overnight at 4°C. Fluorophore-conjugated Odyssey IRDye-680 or IRDye-800 secondary antibody (LI-COR Biosciences, Catalog numbers 926-32211 and 926-68070) was used at 1:10,000 dilution followed by incubation for 1 h at room temperature. Finally, proteins were detected using an Odyssey infrared imaging system (LI-COR Biosciences).

RNA sequencing and analysis
Primary cortical neurons were treated with 2-DG (1mM and 10mM) for 6 h from three independent cultures and RNA was isolated from each sample using a NucleoSpin RNA II Kit (Clontech, Catalog number – 740955-250). For each RNA sample, RNA quality was initially quantified using the RNA Integrity Number (RIN) on an Agilent Bioanalyzer (Agilent Genomics). RNA sequencing was carried out for the RNAs with by the UCLA Neuroscience Genomics Core. In brief, cDNA was generated using Ovation® RNA-Seq System V2 (NuGEN) followed by the library preparation using Illumina's TruSeq Stranded RNA (100ng) + RiboZero Gold. The libraries were pooled and sequenced to generate 75bp paired end reads on HiSeq™4000 system (Illumina). Minimum of 57M reads were obtained. Reads were aligned to the mouse mm10 reference genome using the STAR (ver 2.4.0) spliced read aligner.[78] Uniquely aligned read percentage was 88.09 ± 0.53%(SD). Various quality matrix was generated to use high quality data for the analysis. Read counts for mouse refSeq genes were generated by HT-seq 0.6.1.[79] Genes with at least 5 read events at least half of samples were permitted into the dataset, for a total of 15,787 genes. Raw counts were normalized by trimmed mean of M values (TMM). Differentially expressed genes (DEG) were analyzed using an EdgeR bioconductor R.[80] False discovery rate (FDR) less than 0.1 is used to define differentially expressed genes. Gene Set Enrichment Analysis (GSEA) was performed with gene lists sorted by directional p-Values from differential expression analysis. Raw and processed RNA-seq data are deposited to Gene Expression Omnibus (GEO: GSE217284).

Chromatin immunoprecipitation sequencing (ChIP-seq)
ChIP-seq was performed according to the ChIPmentation protocol with minor modifications. In brief, 40 million primary neurons were used for each condition. Cells were fixed in methanol free formaldehyde (1% final concentration) for 10 min at room temperature with slow rotation to allow the cross-linking of chromatin proteins and DNA. Cross-linking was stopped by incubation with 0.125 M glycine for 5 min at room temperature. The cells were washed twice with ice-cold phosphate-buffered saline (PBS) and 2 ml of cell scrapping solution was added cell were scrapped and collected in respective tubes. Tubes with cells were centrifuged at 2800 rpm for 10 min at 4°C and supernatant was aspirated out. Cell pellets left in the tube were resuspended in 300 μl of 0.25% SDS sonication buffer (10 mM Tris-HCl [pH 8.0], 2 mM EDTA, 0.25% SDS, and protease inhibitor cocktail). The lysates were transferred to 1.5 ml TPX microtubes for sonication (Diagenode, Catalog number: 20190430) and sonicated by Biorupter sonication device (Diagenode) to shear genomic DNA into 200-600 bp fragments. The lysates were centrifuged to remove debris and were then diluted 1:1.5 in equilibration buffer (10 mM Tris-HCl [pH 8.0], 1 mM EDTA, 1.67% Triton X-100, 0.17% sodium deoxycholate, 233 mM NaCl, and protease inhibitor cocktail). Samples were centrifuged again at 14,000 x g, 4 °C for 10 minutes to pellet insoluble material and supernatant was transferred to a new tube. 350 μl of RIPA-LS with added inhibitors was added to the chromatin samples. 600 μl of the chromatin sample was used as I.P. fraction and remaining 45 μl of the chromatin sample was used as input fraction and was preserved at -80°C for use. 15 μg of ATF4 antibody (Millipore, catalog number: ABE387) was added to the I.P. fraction. Both I.P. fraction with added ATF4 antibody and washed Dynabead Protein G (washed with 0.1% BSA/RIPA-LS buffer) were incubated in parallel in separate tubes overnight at 4°C on a rotator with slow rotation. Next day, dynabeads protein G was added to I.P. fraction tube (25μl per sample) and the complex was incubated again at 4°C on a rotator for 2 h with slow rotation. The immuno-complexes were washed twice for 3 min each at 4°C on a rotator with slow rotation with the following buffers: RIPA-low-salt wash buffer (10 mM Tris-HCl [pH 8.0], 1 mM EDTA, 140 mM NaCl, 0.1% SDS, 0.1% sodium deoxycholate, and 1% Triton X-100), RIPA-high-salt wash buffer (10 mM Tris-HCl [pH 8.0], 1 mM EDTA, 500 mM NaCl, 0.1% SDS, 0.1% sodium deoxycholate, and 1% Triton X-100), RIPA-LiCl wash buffer (10 mM Tris-HCl [pH 8.0], 1 mM EDTA, 250 mM LiCl, 0.5% Nonidet P-40, and 0.5% sodium deoxycholate), and TE buffer (10 mM Tris-HCl [pH 8.0] and 1 mM EDTA). Input fraction was thawed on ice. The bead-bound immunoprecipitated DNA and input DNA were tagmented in 25 μl tagmentation reaction containing 5 μl of 5x tagmentation buffer (Illumina, catalog number: 20034210),

19 μl of nuclease free water, and 1 μl of Tn5 (Illumina, catalog number: 20034210) at 37°C for 3 min. Tn5 transposase cleaves double-stranded DNA and ligate adaptors at both ends. Tn5 was inactivated by adding RIPA-LS to the tagmentation reaction and incubating the tube for 5 min on ice. The beads were washed again with RIPA-LS and TE buffer twice each for 3 min at 4°C on a rotator with slow rotation. Beads were then resuspended in 48 μl of ChIP elution buffer (10 mM Tris-HCl [pH 8.0], 5 mM EDTA, 300 mM NaCl, 0.4% SDS, and 2 μl of Proteinase K (Thermofisher Scientific, catalog number: 26160) at room temperature and were incubated at 55°C for 1 h, followed by 65°C incubation for 6 h for reversing the cross-linking and eluting the tagmented DNA. The eluted DNA was purified following SPRI bead cleanup method using AMPureXP beads (Beckman Coulter, catalog number: A63880). To reverse the crosslinking of DNA in input fraction, SDS (0.4% final concentration), NaCl (300 mM final concentration), and 2 μl proteinase K were added into the input sample and the sample was incubated at 55°C for 1 h, followed by 65°C incubation for 6 h. To prepare ChIP and input libraries, tagmented immunoprecipitated DNA and input DNA were amplified by PCR, each with a unique index incorporated. Libraries were selected by size using AMPureXP beads (Beckman Coulter, catalog number: A63880). For high throughput sequencing, DNA libraries were generated using NEBNext® ChIP-seq Library Prep Master Mix Set for Illumina (NEB) and sequenced using an Illumina Novaseq S1 2 x 100bp to obtain an average depth of 50 million of reads per sample. Raw and processed ChIP-seq data are deposited to Gene Expression Omnibus (GEO: GSE217284).

ChIP-seq data analysis
Raw sequencing fastq files were assessed for quality, adapter content and duplication rates with the FastQC, trimmed using trim-galore (https://github.com/FelixKrueger/TrimGalore) and aligned to mouse genome (mm10) with BWA -mem with default parameters.[81] PCR duplicates were removed using Picard MarkDuplicates (https://github.com/broadinstitute/picard) and the bigWig files were created using deepTools[82] with following parameters: bamCompare –binSize 20 –normalized using RPKM. Normalized bigwig files were used to generate heatmaps to visualize sample correlations and to remove outliers. MACS2[83] was used to call narrow peaks with input control with the following command: macs2 call peak -t [ChIP BAM] -c [Input BAM] -f BAMPE -g mm –min-length 100 –q 0.05. We used DiffBind[84] to calculate differences in peak levels between samples. HOMER[60] findMotifsGenome.pl script was used for motif enrichment analysis of differential binding peaks was done by DiffBind (FDR < 0.05). Motif models were drawn from both HOMER and JASPAR database.[85] UCSC genome browser tool was used to compare sequence conservation across different mammalian species.

Electrophysiology
Brains were quickly removed from mice sacrificed by cervical dislocation and placed in cold artificial cerebrospinal fluid (ACSF) (bubbled with 95% O2/5% CO2) containing: 124 mM NaCl, 4 mM KCl, 1 mM Na_2HPO_4, 25 mM $NaHCO_3$, 2 mM $CaCl_2$, 2 mM $MgCl_2$, and 10 mM glucose. The pH and osmolarity of the solution were 7.4 and 310 mOsm/L, respectively. The hippocampus was isolated and placed on a mechanical tissue chopper to produce transverse hippocampal slices of 400 μm thickness. Slices were maintained in a humidified interface chamber at 29 °C and continuously perfused (~1 mL/min) with 95% O2/5% CO2-bubbled ACSF. Hippocampal slices were allowed to recover for at least 90 min prior to beginning the experiment. For recordings, glass electrodes were filled with ACSF and positioned in the CA1 stratum radiatum to record LTP as indicated by Field excitatory post synaptic potential (fEPSPs) evoked by local stimulation (0.1 ms) of Schaffer collateral fibers using a bipolar concentric electrode placed laterally to the recording electrode (~150 μm). For LTP recordings, the voltage intensity of the stimulation test pulse (square pulse, 100 μs duration) for each slice was determined to be the voltage intensity that had generated 30-40% of the maximum slope obtained using input–output relationships. Facilitation was calculated as the ratio of the slopes of the second and first fEPSPs and plotted as a function of the inter-pulse duration. For LTP, a test pulse was applied every minute. Following a steady baseline of 15 min, potentiation was induced with either 100 Hz for 1 s (weak stimulation) or 3 theta-burst stimulations (TBS; 15 s interval), each one involving a single train of 10 bursts at 5 Hz, where each burst is composed of 4 pulses at 100 Hz (strong stimulation). The fEPSP slopes following tetanic stimulation were normalized to the average of the slopes of the fEPSPs acquired during the baseline.

In vivo drug and viral administration
Stereotaxic continuous brain infusion of 2-DG through Alzet mini-osmotic pump implantation
The sterile Alzet mini osmotic pumps (Durect, pump model 1004) were filled with 100 μl of either saline or 2-deoxyglucose (10 μg/μl) and were incubated in saline for 24 h to allow the osmotic release of the drug. Thereafter, the pumps were attached properly with the plastic tubing provided in the brain infusion kit 2 3-5 mm (Durect, catalog number 0008663). We made an intracerebroventricular groove stereotaxically in the mouse brain. We positioned the pump under the skin at the base of the neck and pushed it back toward the left hind limb as far as it went without resistance. We made sure to not let the catheter touch anything. With the curved hemostat, we fixed the cannula at the groove where the top meets the pedestal. We moved the cannula driver into position and secured into place. Then, we used metabond quick adhesive cement system (contains liquid dentin) to seal the cannula on the surface of the skull so that cannula stays there properly for 4-6 weeks. We pushed the top of the cannula into the driver at proper position so that the tubing is pointed straight back. We drove the thin metal catheter through the skull until the plastic cannula base is securely pressed against the top of the skull. The metal catheter can be driven directly through the skull in mice due to the relative thin skull. We pulled any skin that had glue on it away from the skull. With the cannula driver holding the cannula/catheter in place, we waited 1-2 min for the metabond to fully dry. We held the catheter in place with the curved hemostat while raising the driver. Then, we slowly released

the hemostat to ensure that the cannula is properly secured to the skull. With a cotton swab, we pressed down on the top of the cannula. We fitted the clippers into the grove between the top and base of the cannula and clipped off the top of the cannula while still pressing down with the cotton swab. We kept the clippers level so as not to detach the cannula from the skull. If the cannula came unglued, we quickly re-glued with metabond and applied pressure with a cotton swab for an additional 2 min. We closed the opening with clipper and added antibiotic ointment over the head and neck. Thereafter, we unscrewed the ear bars, loosened the nose cone, and removed the mouse from the stereotaxic platform and placed on a warming pad for recovery. We monitored the mice closely for the duration of recovery, typically ranging from 10-30 minutes. We checked every 2-3 minutes until the mouse begins walking around and grooming itself. To control post-operative pain, meloxicam (1-2 mg/kg) was administered subcutaneously, and repeated doses were only administered based on presentation of discomfort/stress in the animals, including hunching, piloerection, vocalization, poor feeding and/or hydration. Animals were monitored daily for the sign of infection at the incision site. We kept the mice back in their respective cages with their proper food and water with 12 h light and dark cycle for four weeks and then proceeded with experiments such as learning and memory related behavior study, LTP study, and gene expression studies.

Intraperitoneal injection of 2-DG

To assess the effect of 2-DG on the *Bdnf* gene expression, mice were injected with either saline or 2-DG (10 mg/kg) i.p. for 6 h and then mice were euthanized properly, and hippocampi were dissected out from mice brain. To assess functional improvement with 2-DG treatment after ischemic stroke, mice were injected with 2-DG (10 mg/kg) i.p. 24 h after induction of the stroke and then every day for four weeks.

Filament MCAO model of ischemic stroke in mouse

The ischemic stroke was induced using filament MCAO method as described before.[58] In brief, all surgeries were conducted in sterile conditions. Male mice were anesthetized with isoflurane (5% induction, and 2% maintenance). A 2 cm incision was opened in the middle of the ventral neck. The right common carotid was temporarily ligated with 6-0 silk (Ethicon Inc.). Right unilateral MCAO was accomplished by inserting a Silicon rubber-coated monofilament (Doccol Corporation) into the internal carotid artery via the external carotid artery stump and common carotid artery. Adequacy of MCAO was confirmed by monitoring cortical blood flow at the onset of the occlusion with a laser Doppler flowmetry probe affixed to the skull (Periflux System 5010; Perimed, Sweden). Animals were excluded if mean intra-ischemic laser Doppler flowmetry was >30%pre-ischemic baseline. Transient focal cerebral ischemia was induced in mice for 60 minutes by reversible MCAO in the right brain hemisphere under isoflurane anesthesia followed by 24 h of reperfusion. Body temperature was controlled at 36.5 ± 0.5_C throughout MCAO surgery with warm water pads and a heating lamp. After 60 minutes of occlusion, the occluding filament was withdrawn to allow for reperfusion and the incision was closed with 6-0 surgical sutures (ETHICON,Inc). After surgery, 0.5 ml pre-warmed normal saline was given subcutaneously to each mouse. Mice were then allowed to recover from anesthesia.

Stereotaxic intracerebroventricular administration of 2-DG

Using a nanomite syringe pump and Hamilton syringe, 5 μl of either saline or 2-DG (1 μg/μl) was infused directly into the ventricles at a rate of 0.120 ml/min in mice, which were injected with AAV8-CMV- 5'UTR ATF4 luciferase intracranial double injection three weeks before. The injection site relative to the bregma point was lateral, 0.05; anteroposterior, 0.12 and dorsoventral, 0.25. Surgeon was blinded to treatment and control groups.

In vivo bioluminescence imaging

To assess the induction of ATF4 with 2-DG treatment, we injected AAV8 viral vector expressing CMV-5'UTR from the ATF4 gene tagged with luciferase through intracranial double injection and allowed maximal expression for three weeks and then injected either saline or 25 μg of 2-DG (1 mg/kg) intracerebroventricularly (i.c.v.) for 4 h. Thereafter, mice were placed in the In Vivo Imaging System (IVIS; PerkinElmer) induction chamber and anesthetized with isoflurane (3 to 4% with an oxygen flow of 1 liter/min). The mice were individually removed from the induction chamber and given an i.p. injection of D-luciferin (150 mg/kg; Promega) suspended in sterile saline (Invitrogen). After a 10 min incubation period, the mice were placed on the imaging platform of the IVIS Spectrum imaging station supplied with isoflurane at 1.5% with an oxygen flow of 1 liter/min during the imaging procedure. White light and luciferase activity images were obtained at 30-s intervals for 5 min. After imaging, the mice were removed from the imaging stage and were allowed to recover in a heated cage. Images were analyzed to quantify luminescence in either the brain or liver using Living Image software (PerkinElmer). The images were assessed by the quantitative measurement of the luminescence intensity from the pseudo-colored bioluminescence.

Assessment of urine ketone body and other physiological parameters

Urine ketone body was measured using Ketofax reagent strips (Smackfat, USA). Body weight was measured using Electronic Top loading Balance (Thomas Scientific, Switzerland). Body temperature was measured through rectal temperature using digital thermometer (Harvard Apparatus, USA). To take the temperature, mice were guided to walk into the restraint tubes and their excessive movement was controlled by adjusting the tube end holders. The blood pressure and heart rate were assessed using the CODA Monitor noninvasive blood pressure acquisition system for mice (Kent Scientific, Torrington, CT). Blood pressure is detected by this system based on volume changes in the tail. Mice acclimatized for a 1-hour before starting the experiment in a quiet area

(22 ± 2°C). The occlusion cuff was fitted close to the base of the tail and the VPR sensor cuff was kept next to the occlusion cuff. Mice were warmed for 5 minutes on heating pads preheated to 33 to 35°C before and during blood pressure recordings. The occlusion cuff is inflated to 250 mmHg and deflated over 20 s for blood pressure measurement. Blood oxygen saturation and heart rate were measured using MouseSTAT

Pulse Oximeter & Heart Rate Monitor (Kent Scientific, Torrington, CT). Blood glucose was measured using GE100 Blood Glucose Monitor (Ontario, CA) in a drop of blood collected from tail puncture.

Behavioral analysis
Corner turn test
The integrated sensorimotor function in both stimulation of vibrissae (sensory neglect) and rearing (motor response) was assessed through the corner turn test as described previously.[52] Mice were placed between two cardboard pieces forming a corner with a 30° angle. While maintaining the 30° angle, the boards were gradually moved toward the mouse until the mouse approached the corner, reared upward, and turned 180° to face the open end. The direction (left or right) in which the mouse turned around was recorded for each trial. Ten trials were performed for each mouse.

Adhesive tape removal task
The adhesive tape removal task in mice was performed as previously described.[52] Briefly, adhesive tape was placed on the planter region of the forward paw (right and left) of mice. The time from which the tape was applied to when the mouse successfully removed it was recorded for each paw. A maximum of 300 s for each paw was allowed.

Pole test
The Pole test assesses motor function. Pole test as performed as previously described.[88] Animals were placed on top of a 50- to 55-cm vertical pole with a diameter of 8 to 10 mm and were trained to descend the pole with their snouts facing downward. Scoring started when the animal initiated the turning movement. The latency to reach the ground were recorded. However, if an animal fell immediately or stopped descending, the trial was excluded and repeated. The surface of the pole was made rough with adhesive tape to avoid sliding.

Spontaneous alternation test (Y-maze test)
Short term spatial memory was assessed by testing spontaneous alteration behavior in the Y-maze. Mouse prefers to explore a new arm of the Y-maze instead of coming back to the previous arm, which was already visited. Y-maze has three equal arms each spaced at 120 degrees with respect to other arms. Recording of the testing began with the release of mouse in one arm and the mouse was allowed to explore in different arms of the maze for 8 min. The sequence and the total number of arm entries were recorded. The mouse was within one arm when paws of the mouse were completely in that arm. An alternation was considered complete when mouse entered in all three arms in a consecutive manner. The number of total alternation was calculated as the total number of arm entries minus 2 and the percentage of alternation was calculated as (actual alternation/total number of entries) x 100.

Morris water maze test
Spatial learning and memory were analyzed using the Morris water maze. The mice were handled daily, starting 1 week before behavioral testing, to habituate them. During the acquisition period, visual cues were arranged in the four corners of the tank. The hidden platform was in the middle of the northwest quadrant. Each day, mice were placed next to and facing the wall of the basin in four starting positions: north, east, south, and west, corresponding to four successive trials per day. The duration of a trial was 90 sec. Whenever the mouse failed to reach the platform within 90s, it was placed on the platform by the experimenter for 10 sec. Latencies before reaching the platform were recorded for 7 days and analyzed. A probe trial was assessed 24 h after the last trial of the acquisition period by removing the platform from the pool. Mice were released on the north side for a single trial of 90 sec, during which the time spent around the platform was measured. Latencies before reaching the platform were recorded and averaged.

QUANTIFICATION AND STATISTICAL ANALYSIS

All experiments were performed as at least three independent sets and data were presented as means ± SD or means ± SEM. Statistical significances were assessed using GraphPad Prism using either Student's t tests to compare values between two specific groups or one-way ANOVA followed by Dunnett's post-hoc test/Tukey's Post-hoc test/Bonferroni Post-hoc test to compare the values of more than two groups or two-ANOVA with Tukey's multiple comparisons test/Šidák's multiple comparisons test/Bonferroni post-hoc test to compare two or more than two groups at a particular time point or Repeated Measures two-way ANOVA with Tukey's multi-comparison test/Fisher's LSD post-hoc test to compare the values of two or more than two groups at different time points. Statistical details for each figure can be found in the respective figure legend. The p value of 0.05 or less was considered statistically significant in all statistical analyses. For all AD and stroke in vivo studies, power calculation was done by an unpaired t-test and each group had > 80% power at alpha level of 0.05.